



**NAVAL
POSTGRADUATE
SCHOOL**

MONTEREY, CALIFORNIA

THESIS

CONTACT ANALYSIS OF NOMINALLY FLAT SURFACES

by

Matthew R. Shellock

June 2008

Thesis Advisor:

Young W. Kwon

Approved for public release; distribution is unlimited.

THIS PAGE INTENTIONALLY LEFT BLANK

REPORT DOCUMENTATION PAGE			<i>Form Approved OMB No. 0704-0188</i>	
Public reporting burden for this collection of information is estimated to average 1 hour per response, including the time for reviewing instruction, searching existing data sources, gathering and maintaining the data needed, and completing and reviewing the collection of information. Send comments regarding this burden estimate or any other aspect of this collection of information, including suggestions for reducing this burden, to Washington headquarters Services, Directorate for Information Operations and Reports, 1215 Jefferson Davis Highway, Suite 1204, Arlington, VA 22202-4302, and to the Office of Management and Budget, Paperwork Reduction Project (0704-0188) Washington DC 20503.				
1. AGENCY USE ONLY (Leave blank)	2. REPORT DATE June 2008	3. REPORT TYPE AND DATES COVERED Master's Thesis		
4. TITLE AND SUBTITLE Contact Analysis of Nominally Flat Surfaces			5. FUNDING NUMBERS	
6. AUTHOR(S) Shellock, Matthew R.				
7. PERFORMING ORGANIZATION NAME(S) AND ADDRESS(ES) Naval Postgraduate School Monterey, CA 93943-5000			8. PERFORMING ORGANIZATION REPORT NUMBER	
9. SPONSORING /MONITORING AGENCY NAME(S) AND ADDRESS(ES) N/A			10. SPONSORING/MONITORING AGENCY REPORT NUMBER	
11. SUPPLEMENTARY NOTES The views expressed in this thesis are those of the author and do not reflect the official policy or position of the Department of Defense or the U.S. Government.				
12a. DISTRIBUTION / AVAILABILITY STATEMENT Approved for public release; distribution is unlimited.			12b. DISTRIBUTION CODE	
13. ABSTRACT (maximum 200 words) A proper understanding of the mechanism of contact between two or more nominally flat surfaces is crucial in the design process of many devices. This thesis, using analytical and computational methods, models the former through the use of fractal characteristics at the contact interface. A parametric analysis of the fractal surface was completed in order to properly understand fractal geometry and its effect on surface properties. The fractal surface was simplified so that Hertz theory could be used to model surface deformation and resulting contact stresses. The data gathered from the model was then input into an existing electromagnetic rail gun program to study the contact surface effect on exit velocity, temperature, electrical conductivity, and contact area ratio. Finally, a study of the fractal parameter effects on the electromagnetic rail gun was completed.				
14. SUBJECT TERMS Hertz, interface, contact, stress, deformation, fractal, electromagnetic rail gun			15. NUMBER OF PAGES 69	
			16. PRICE CODE	
17. SECURITY CLASSIFICATION OF REPORT Unclassified	18. SECURITY CLASSIFICATION OF THIS PAGE Unclassified	19. SECURITY CLASSIFICATION OF ABSTRACT Unclassified	20. LIMITATION OF ABSTRACT UU	

NSN 7540-01-280-5500

Standard Form 298 (Rev. 2-89)
Prescribed by ANSI Std. Z39-18

THIS PAGE INTENTIONALLY LEFT BLANK

Approved for public release; distribution is unlimited.

CONTACT ANALYSIS OF NOMINALLY FLAT SURFACES

Matthew R. Shellock
Lieutenant, United States Navy
B.S., United States Naval Academy, 2001

Submitted in partial fulfillment of the
requirements for the degree of

MASTER OF SCIENCE IN MECHANICAL ENGINEERING

from the

NAVAL POSTGRADUATE SCHOOL
June 2008

Author: Matthew R. Shellock

Approved by: Young W. Kwon
Thesis Advisor

Anthony J. Healey
Chairman, Department of Mechanical and Astronautical
Engineering

THIS PAGE INTENTIONALLY LEFT BLANK

ABSTRACT

A proper understanding of the mechanism of contact between two or more nominally flat surfaces is crucial in the design process of many devices. This thesis, using analytical and computational methods, models the former through the use of fractal characteristics at the contact interface. A parametric analysis of the fractal surface was completed in order to properly understand fractal geometry and its effect on surface properties. The fractal surface was simplified so that Hertz theory could be used to model surface deformation and resulting contact stresses. The data gathered from the model was then input into an existing electromagnetic rail gun program to study the contact surface effect on exit velocity, temperature, electrical conductivity, and contact area ratio. Finally, a study of the fractal parameter effects on the electromagnetic rail gun was completed.

THIS PAGE INTENTIONALLY LEFT BLANK

TABLE OF CONTENTS

I.	INTRODUCTION.....	1
	A. MOTIVATION	1
	B. BACKGROUND AND LITERATURE SURVEY.....	2
	1. Greenwood and Williamson.....	2
	2. J. F. Archard	3
	3. Yan and Komvopoulos	4
	4. Sahoo and Ghosh	5
	5. Ali and Sahoo.....	6
	6. Pratikakis.....	7
	7. Polonsky and Keer	8
	8. Hu, Panagiotopoulos, Panagouli, Scherf, and Wriggers	9
	C. OBJECTIVE	9
II.	FRACTAL SURFACES.....	11
	A. FRACTAL REPRESENTATION	11
	B. CREATION OF BASELINE FRACTAL SURFACE.....	11
	C. PARAMETRIC STUDY	13
	1. Variation of the Number of Superposed Fractal Ridges, M	13
	2. Variation of the Fractal Roughness, G	15
	3. Variation of the Fractal Dimension, D	17
	4. Variation of the Density of the Profile Frequency, γ	19
III.	CONTACT MODELING.....	23
	A. FORCE-DEFLECTION MODELING	23
	1. Hertz Equations	23
	2. MATLAB Program.....	24
	3. Results, Deflection-Generated Opposition Pressure.....	26
	a. Variation of the Number of Superposed Fractal Ridges, M	26
	b. Variation of the Fractal Roughness, G	28
	c. Variation of the Fractal Dimension, D	29
	d. Variation of the Density of the Profile Frequency, γ	30
	4. Results, Deflection-Generated Contact Area Ratio	31
	a. Variation of the Number of Superposed Fractal Ridges, M	31
	b. Variation of the Fractal Roughness, G	32
	c. Variation of the Fractal Dimension, D	33
	d. Variation of the Density of the Profile Frequency, γ	34
	5. Curve Fitting	35
V.	RAIL-GUN MODELING AND ANALYSIS.....	37
	A. INTRODUCTION.....	37
	B. PRATIKAKIS MODEL	37

1.	Part I, Setup of Inertial Coordinate System and Geometric Configuration	37
2.	Part II, Main Program and Description of Functions	37
C.	RESULTS OF MODIFIED PRATIKAKIS EQUATION.....	39
1.	Variation of the Number of Superposed Fractal Ridges, M	39
2.	Variation of the Fractal Roughness, G	40
3.	Variation of the Fractal Dimension, D	42
4.	Variation of the Density of the Profile Frequency, γ	43
VI.	SUMMARY AND CONCLUSIONS	47
VII.	RECOMMENDATIONS.....	49
	LIST OF REFERENCES.....	51
	INITIAL DISTRIBUTION LIST	53

LIST OF FIGURES

Figure 1.	Rail Gun Structure [1].....	1
Figure 2.	Baseline Fractal Surface.	13
Figure 3.	Fractal Surface; Increased M	14
Figure 4.	Fractal Surface; Decreased M	15
Figure 5.	Fractal Surface; Increased G	16
Figure 6.	Fractal Surface; Decreased G	17
Figure 7.	Fractal Surface; Increased D	18
Figure 8.	Fractal Surface; Decreased D	19
Figure 9.	Fractal Surface; Increased γ	20
Figure 10.	Fractal Surface; Decreased γ	21
Figure 11.	Pressure-Deflection Curves, Changing Parameter M	27
Figure 12.	Pressure-Deflection Curves, Changing Parameter G	28
Figure 13.	Pressure-Deflection Curves, Changing Parameter D	30
Figure 14.	Pressure-Deflection Curves, Changing Parameter γ	31
Figure 15.	Area Ratio-Deflection Curves, Changing Parameter M	32
Figure 16.	Area Ratio-Deflection Curves, Changing Parameter G	33
Figure 17.	Area Ratio-Deflection Curves, Changing Parameter D	34
Figure 18.	Area Ratio-Deflection Curves, Changing Parameter γ	35
Figure 19.	Polynomial Curve-Fitting.	36
Figure 20.	Schematic of Rail Gun Program [8].....	38
Figure 21.	Variation of the Number of Superposed Fractal Ridges, M	40
Figure 22.	Variation of the Fractal Roughness, G	41
Figure 23.	Variation of the Fractal Dimension, D	43
Figure 24.	Variation of the Density of the Profile Frequency, γ	44

THIS PAGE INTENTIONALLY LEFT BLANK

LIST OF SYMBOLS

x, y, z	Cartesian coordinates
G	Fractal roughness, a height-scaling parameter
L	Fractal cut-off length
D	Fractal dimension
γ	Density of the profile frequency
M	Number of superposed fractal ridges
ϕ	Random phase angle
r	Peak radius
a	Hertz radius
P	Contact force
σ_c	Contact pressure
E	Young's modulus or elastic modulus
δ	Contact deflection length
A	Contact area

THIS PAGE INTENTIONALLY LEFT BLANK

ACKNOWLEDGMENTS

To my parents

THIS PAGE INTENTIONALLY LEFT BLANK

I. INTRODUCTION

A. MOTIVATION

In order to properly develop the technology used in the electromagnetic rail gun, one must take into consideration the importance of the contact mechanics involved. Mechanical, thermal, and electrical contact must all be understood at the interface between rail and armature. Figure 1 below displays a generic view of current rail gun construction.

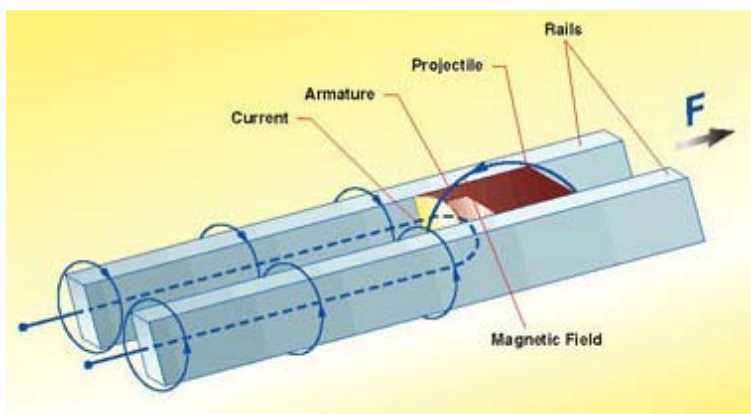


Figure 1. Rail Gun Structure [1].

The contact surface between the armature and the rails is an area that has been a problem for the development of the rail gun due to the simple fact that for proper operation, electrical contact must remain consistent throughout a firing. As the rail gun armature moves down the rails, the contact surface changes, and often results in changes in electrical contact. Issues arise when the surface profile changes enough so that an arc occurs. This arc causes a rapid increase in resistive heating well above the metals vaporization temperature which results in significant erosion [1].

This thesis investigates the mechanics of contact at the microscopic level so that a better understanding of the properties of nominally flat surfaces may be improved. Using the commercial computer program MATLAB, the mechanics of contact will be modeled and tested with the hopes of future improvements to the electromagnetic rail gun and similar defense-related issues.

B. BACKGROUND AND LITERATURE SURVEY

The first well-documented study of contact was that of Heinrich Rudolf Hertz in 1881. The well known Hertz problem is one in which the contact stresses are solved for the simple cases of a sphere on a plane, a sphere on a sphere, and a cylinder on a cylinder; all perfect geometry [2]. Because Hertz theory is applicable for simple cases, many scientists in more recent history have developed more robust methods for solving contact problems.

1. Greenwood and Williamson

The goal of this research was to investigate the contact of nominally flat (but microscopically rough) surfaces. The assumption of nominally flat is defined as those surfaces in which the area of apparent contact is large so the individual contacts are dispersed and do not influence the neighboring contact locations. The purpose was to describe the theory of elastic contact and how it was closely related to real surfaces than the earlier theories. In order to compare the theoretical results, statistical results were tabulated and presented.

A mathematical model was created to analyze the simple case of Hertz-contact (a spherical body in contact with a rigid flat plane) and determine the change in contact area with varying load. The mathematical model was then compared to experimental results to compare the change of pressure with different loads. Contact was then related to material hardness to compare the actual deformation with different loads. The development of a Taylor-Hobson model 3 Talysurf allowed the authors to analyze the surface topography of common materials. The research went on to describe the mechanics of material wear.

Due to the fact that this research was completed in 1966, modern methods of calculation and computer-aided solvers were unavailable. The methodology began with the previous theory of Hertz contact and developed a surface model to analytically solve for deformation and area change with increased forces. Comparisons were made with

experimental results. Also, statistical tabulation of the real surface profiles allowed the scientists to justify their assumptions of nominally flat surfaces as normal in most contact.

The biggest conclusion of the research was that the separation between two surfaces depends on the nominal pressure (load divided by contact area), the number of micro-contacts and the total area of contact depend on the load only. These authors also developed the concept of “elastic hardness”, or basically that the area of contact can be predicted from the load the same way that it is for plastic contact using the conventional data for material hardness. They also discovered that most common surfaces have a Gaussian distribution of asperity heights [3]. The data gathered by these authors was cited as a reference for all of the other researchers mentioned in this thesis.

2. J. F. Archard

The purpose of this research was to investigate the hypothesis that elastic deformation of surface protuberances (asperities) was consistent with Amonton’s law, that the friction is proportional to the applied load. The basic idea investigated was that friction between sliding surfaces arises from local adhesion at the regions where protuberances come into real or molecular contact.

Using Amonton’s law as a starting point, the author developed the theory of multiple small contacts in friction and backed up his results with experiments. The focus of the research was in the experimentation using a crossed-cylinders friction machine and the high polymer Perspex as the test material. Perspex was used due to its high capability to sustain large deformations under elastic conditions. The experimental results were used to develop coefficients of static friction based upon overall compressive load. Additional experiments were performed to analyze wear due to friction. The aforementioned experiments were redone using metal specimens and compared to the hypothesis that elastic deformation was the primary cause of change and not plastic deformation.

Similar to Greenwood & Williamson, the author had limited computing power, and thus his work focused on experiments and tabulated results. Much of the research

focused on experimental setup, which required great precision in order to gather sufficient accurate results. The results of the experiments were compared to Amonton's law of friction and results justified.

The major conclusion from the research was that the real area of contact formed between two sliding surfaces was due to elastic deformation of the contacting protuberances. It was shown that the aforementioned assumption was consistent with Amonton's law of friction. The conclusion was valid for both Perspex (with a large elastic range) and for carefully prepared metals under conditions where the damage was small [4].

3. Yan and Komvopoulos

The goal of this research was to introduce a comprehensive contact mechanics analysis of elastic-plastic rough surfaces that can be characterized by three-dimensional fractal geometry and to present numerical results revealing the variation of the interfacial contact force and real contact area during quasistatic surface approach.

The fractal surface equation was developed using the fractal geometry. Fractal geometry is common in nature, and can be observed in turbulence, precipitation, and specifically surface topography. Starting with the Weierstrass-Mandelbrot Equation (fractal equation), the engineers approximated the power spectrum, and generalized the equation using proper scaling properties. By including a random phase into the equation, they were able to develop a 3-dimensional function of x and y to create a surface with a fractal profile. Using this fractal profile, Hertz contact analysis was performed, with the major assumption that the contact areas could be modeled as individual spheres. Stress-Strain curves were used to model the elastic-plastic transformation. The numerical results were summarized to reveal the effect of material behavior on the resulting contact force. Graphs of the aforementioned numerical data were included.

The methodology used in this research was a combination of 3 major areas. First, the overall approach was one that generated surface profiles using fractal mechanics. Using the fractal approach gave the authors the ability to randomly change the surface profile easily. The next major area was in the Hertz Contact Theory. This area, though

full of assumptions, was the focus of analyzing the actual contact between the two surfaces. Last, the results were compared statistically to ensure that the results were within the realm of actually observed experimental results.

The research analyzed elastic-plastic rough surfaces characterized by 3-dimensional fractal geometry. The theoretical analysis of total contact force and real contact area in terms of surface separation distance, fractal parameters, and material properties helped to further develop insight into the effects of surface topography on contact. It was found that the actual contact area for elastic-plastic rough silica surfaces [the ones analyzed] was a remarkably small fraction of the apparent contact area, thus for most of the range of surface separation, the predominant deformation and resulting contact was due to elastic effects [5].

The research conducted by Yan and Komvopoulos was very much on the cutting edge of current contact research. The fractal approach was actually a major motivating factor for the research developed in this thesis.

4. Sahoo and Ghosh

The goal of this research was to use the finite element method to model the contact between 3-dimensional surfaces with fractal geometry. The focus was on developing non-dimensional contact area and displacement as functions of non-dimensional load for different surface profiles in the case of elastic contact. Also analyzed was the effect of strain-hardening in the case of elastic-plastic contact.

Similar to the research of Yan and Komvopoulos, the Weierstrass-Mandelbrot function was used to model the surface topography. A finite element analysis was performed using the commercial software program ANSYS, which calculated the contact area after application of the load. A test of the finite element model was used with the simple sphere in contact with a rigid flat plane to ensure that the model could accurately determine the case of Hertz contact, which had already been completed experimentally. Both the analytical and FEM solutions were compared and solutions were generated for elastic contact and elastic-plastic contact.

The methodology used by Sahoo and Ghosh was a combination of 4 major areas of research. First, the overall approach was one that generated surface profiles using fractal mechanics. Using the fractal approach gave the authors the ability to randomly change the surface profile easily. The next major area was in the Hertz Contact Theory. This area allowed the authors to develop an analytical solution. The third major area was in the use of the finite element method and commercial, off the shelf program [ANSYS] to develop a solution. The fourth, and possibly most important area of research, was the development of the solutions using non-dimensional methods which allowed their model to be independent size, scaling all numbers properly.

The results of the FEM analysis agreed with the experimental results that were tabulated in previous literature. They discovered that in the elastic regime, contact area was linearly proportional to the contact load at small loads, but at high loads, the behavior became nonlinear. In the case of elastic-plastic contact, similar results were found. The system was linear for small loads, and nonlinear for larger loads with a direct effect on strain hardening [6].

This research is on the cutting edge of current contact analysis research. The fractal geometry matches nature closely, and can easily be scaled non-dimensionally. Of note by Sahoo and Ghosh, is that their solution is highly dependent on an accurate development of the true surface profile. Without knowing the specific details of the surface one is analyzing, the proper fractal surface can not be developed for accurate research.

5. Ali and Sahoo

The purpose of this research was to describe the adhesive contact between rough surfaces with small-scale surface asperities using an elastic-plastic model of contact deformation based on fictitious plastic asperity concept developed by other researchers, Abdo and Farhang [7]. The work began with a literature survey which discussed the work of Greenwood and Williamson and the downfalls of Hertz-contact assumptions.

The topic of adhesion contact and the Tabor number (the ratio of elastic deformation to the range of action of adhesion forces) was introduced. The idea that the earlier analyses of adhesive contact treated everything on the macroscopic level as elastic-plastic, but at the microscopic level, the deformation of asperities was elastic then perfectly plastic. The concept of elastic-plastic adhesive forces was developed using the plastic asperity concept. Using a mathematical model, Ali and Sahoo were able to investigate three different asperity deformation conditions: purely elastic, elastic-plastic, and purely plastic. The results were solved and presented in graphical format.

This modern approach to solving the elastic-plastic adhesive contact between two forces is at the forefront of using the computational method to solving difficult problems. Significant research was accomplished to investigate the shortcomings of prior research in order to develop a program that would solve for the details of different cases of deformation. Basically, where previous researchers assumed either plastic or elastic, Ali and Sahoo developed a program that could test the entire span of deformation.

The results of the program were conclusive, and the prediction of load-separation behavior of contacting rough surfaces as functions of well-established elastic adhesion index and plasticity index. Basically, the results took previously tabulated material properties, which gave them the ability to analyze elastic and plastic behavior on both the macroscopic (material) and the microscopic (asperities on the surface). The representation of the data claimed to be a more-realistic model than all previous [8].

This research is the most current and up-to-date use of computing power to solve a problem that had previously been modeled. By taking known data for elastic or plastic contact and solving for the grey area in between, the authors created a program that is the most accurate representation of the real world. One suggestion that could be made for future work would be the inclusion of a graphical 3-D model in order to compare it to experimental deformation.

6. Pratikakis

The research of Nikolaos Pratikakis for his Master's thesis was to develop a mathematical program to model the electromagnetic rail gun. His research used the finite

element method to solve for the potential field, temperature field, stress field, electrical conductivity, and thermal conductivity between the rails and the armature. His program used statistical data from experimentally gathered topographical data for typical rail and armature surfaces to model the contact interface. Using known analytical formulae for the multi-physics situation that develops within the rail gun, he was able to use the finite element method to determine the characteristics of the rail and armature during the entire cycle of a firing [9].

The Pratikakis program is used in this thesis to determine the properties of the rail gun when the armature and projectile exit the rails. His method was altered to account for fractal geometry at the interface between the rails and armature, but his finite element method solver was left as is. Using Pratikakis' method, the thesis research conducted herein could be expanded for the application to the electromagnetic rail gun.

7. Polonsky and Keer

The purpose of the research completed by Polonsky and Keer was to develop a faster way to solve rough contact problems. Arguing that the Hertz theory uses the stress-displacement response of individual microcontacts and does not take into account the effects of neighboring contact points, they sought to develop a method that would accurately describe generalized contact.

The method that Polonsky and Keer adopted was the multi-level multi-summation and conjugate gradient techniques. They determined the real contact area using the conjugate gradient method. Then, using a two-dimensional multi-level multi-summation algorithm, they were able to keep the summation error under the discretization error. Their method views the contact surface as a three-dimensional grid in contact with another surface that has the same number of nodes on its respective grid. Assuming that the contact planes remain parallel to one another, their algorithm solves the three-dimensional general grid and then simplifies that grid into a two-dimensional grid that only represents the contact regions. Thus, their method is quick and accurate, taking into account the effects of regional contact points on one another [10].

This method takes into account regional contact effects on one another, but does so using purely elastic theory. It also models the contact as two dry surfaces in rough contact, which may or may not be the proper case in many lubricated mechanical devices. Further research and development would be helpful to develop a mathematical solver that takes into account lubrication, elastic-plastic deformation, and stress-strain relationships within the contact surface.

8. Hu, Panagiotopoulos, Panagouli, Scherf, and Wriggers

The objective of the research of Hu, Panagiotopoulos, Panagouli, Scherf, and Wriggers was to develop a program in which real contact areas could be found accurately using the finite element solution. Additionally, they sought to minimize computational costs while retaining accuracy. An adaptive finite element method was used to model fractal interfaces in a contact problem with the assumption of linear and finite elasticity. The focus on the research was in the problem description and the formulation of fractal interfaces. Contact kinematics was based upon different penetration characteristics when two different bodies came into contact with one another. This research concluded with the development and testing of the Finite Element Analysis Program (FEAP) using linear triangular elements [11].

The results and visual graphics of the developed program were similar to the commercial finite element program, ANSYS. Future development and research are recommended to improve the current program and allow for multiple types of contact to include elastic-plastic and friction.

C. OBJECTIVE

The objective of this research is to develop a mathematical model to determine the contact stresses between nominally flat surfaces. This situation is found in countless engineering applications, and is one of the prime factors in the development of the electromagnetic rail gun. By using simple Hertz theory applied to the complex geometry of a fractal surface, the intention is to create a simple model which will allow designers to choose different surface topographies and material properties during the development of the rail gun. The model developed will be an analytical model, strictly using

mathematics and computational analysis to determine contact stresses and area changes due to mechanical contact between two nominally flat surfaces. The commercial program MATLAB 7.2 will be used to develop all computer code. All assumptions will be clearly stated in appropriate sections.

II. FRACTAL SURFACES

A. FRACTAL REPRESENTATION

The concept of “fractal dimension” was introduced by the mathematician Felix Hausdorff in 1918. This concept, distinct from the simple figures of Euclidean geometry was coined “fractal” by Benoit B. Mandelbrot of Poland. Mandelbrot was the first to point out the feasibility of modeling natural, physical objects with the concept. The property of self-similarity, which describes a system whose component parts represent the entirety of the system, make fractals an excellent choice for modeling surface topographies. Fractals remain invariant under changes of scale. The fractal concept has been adopted and used by mathematicians and engineers since 1975 [12]. The application of fractal geometry is applied hereafter to model physical topography with seemingly random features.

B. CREATION OF BASELINE FRACTAL SURFACE

The first step in modeling the fractal surface was to use the following fractal surface equation developed by Yan and Komvopoulos [5]:

$$\begin{aligned}
 z(x, y) = & L \left(\frac{G}{L} \right)^{(D-2)} \left(\frac{\ln \gamma}{M} \right)^{1/2} \sum_{m=1}^M \sum_{n=0}^{n_{\max}} \gamma^{(D-3)n} \\
 & \times \left\{ \cos \phi_{m,n} - \cos \left[\frac{2\pi\gamma^n (x^2 - y^2)^{1/2}}{L} \right. \right. \\
 & \left. \left. \times \cos \left(\tan^{-1} \left(\frac{y}{x} \right) - \frac{\pi m}{M} \right) + \phi_{m,n} \right] \right\}
 \end{aligned} \tag{1}$$

To establish a baseline plot of the surface, MATLAB 7.2 was used with the following quantities substituted into the above equation:

$L = 1.0 \times 10^{-8}$ (m)	$\gamma = 1.5$	$\phi = 5.9698$ (rad)	(2)
$G = 1.36 \times 10^{-11}$ (m)	$M = 10$		
$D = 1.2$	$n_{\max} = 100$		

MATLAB code was developed to solve for the magnitude of z over a domain of one micrometer in the x and y directions, respectively. These heights, obtained by the equation for $z(x, y)$ above, were then plotted using the embedded MATLAB code *surf*. This code creates a mesh plot with the spaces between the lines, called patches, filled in according to a color scheme based on the z data.

In order to provide a cutaway view of the surface, the equation for $z(x, y)$ was simply modified. The value of y was held constant, arbitrarily at 50 nanometers, to display the profile in the middle of the sample. The values of z were then displayed using the MATLAB code *plot*. The results of these calculations are shown below as Figure 2. This two-dimensional profile more clearly shows the distribution of peaks and valleys in the domain. Of note is the randomness of the peak height distribution throughout the sample.

MATLAB code was then developed to determine the location of the local peaks of the plotted surface. A peak was defined as a specific point whose value for z was larger than both the preceding and following value of z in the x and y directions. The height of the peak, or z value, was then saved into a column vector for further calculations. Using this column vector, the peak radius was then solved for at each location deemed a peak. To solve for the peak radius, it was assumed that this radius was equal to the radius of curvature at the location of the peak. This was solved by setting the radius of curvature equal to the reciprocal of the second derivative as shown below:

$$r = \left| \frac{(\Delta x)^2}{z_{(x+1)} + z_{(x-1)} - 2z_{(x)}} \right| \quad (3)$$

This equation was solved in both the x and y directions, and then averaged to find the overall peak radius at that location. Although averaging in only the x and y directions may not be the most accurate assumption, it was used to simplify the calculations.

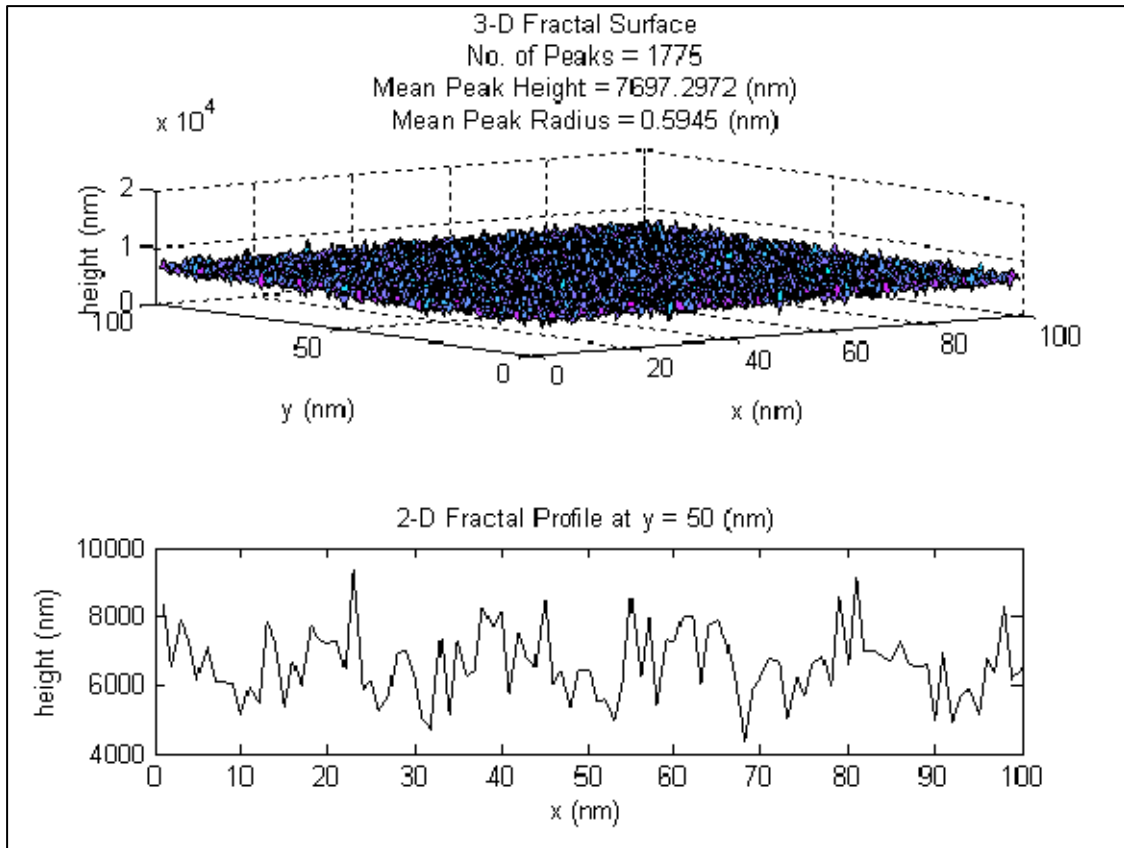


Figure 2. Baseline Fractal Surface.

In order to gain a better understanding of the effects each parameter has on the surface profiles, the values for each of the variables in the z equation were varied. The following sections discuss the different parameters of the equation while displaying the results when each variable is increased and decreased from the baseline value. Included in the MATLAB plot were the mean peak height and mean peak radius over the domain shown. These values were calculated and displayed to assist in discerning between the different parameter changes.

C. PARAMETRIC STUDY

1. Variation of the Number of Superposed Fractal Ridges, M

The parameter M in the equation for z in terms of fractal notation represents the number of superposed fractal ridges. This parameter, if set equal to one, would construct a cylindrical, corrugated, two-dimensional surface. Thus, for values greater than one, the

parameter controls how many ridges are present in the surface. Figure 3 displays the fractal surface and profile when M is increased from the baseline value of 10 to 12. The change of M results in an increased total number of peaks over the domain, specifically from 1775 to 1835. The mean peak height increased, from approximately 7697 to 8601 nanometers. Conversely, the mean peak radius is reduced from 0.59 to 0.18 nanometers. Thus, the peaks on average have increased height and decreased in radius, giving higher, narrower peaks.

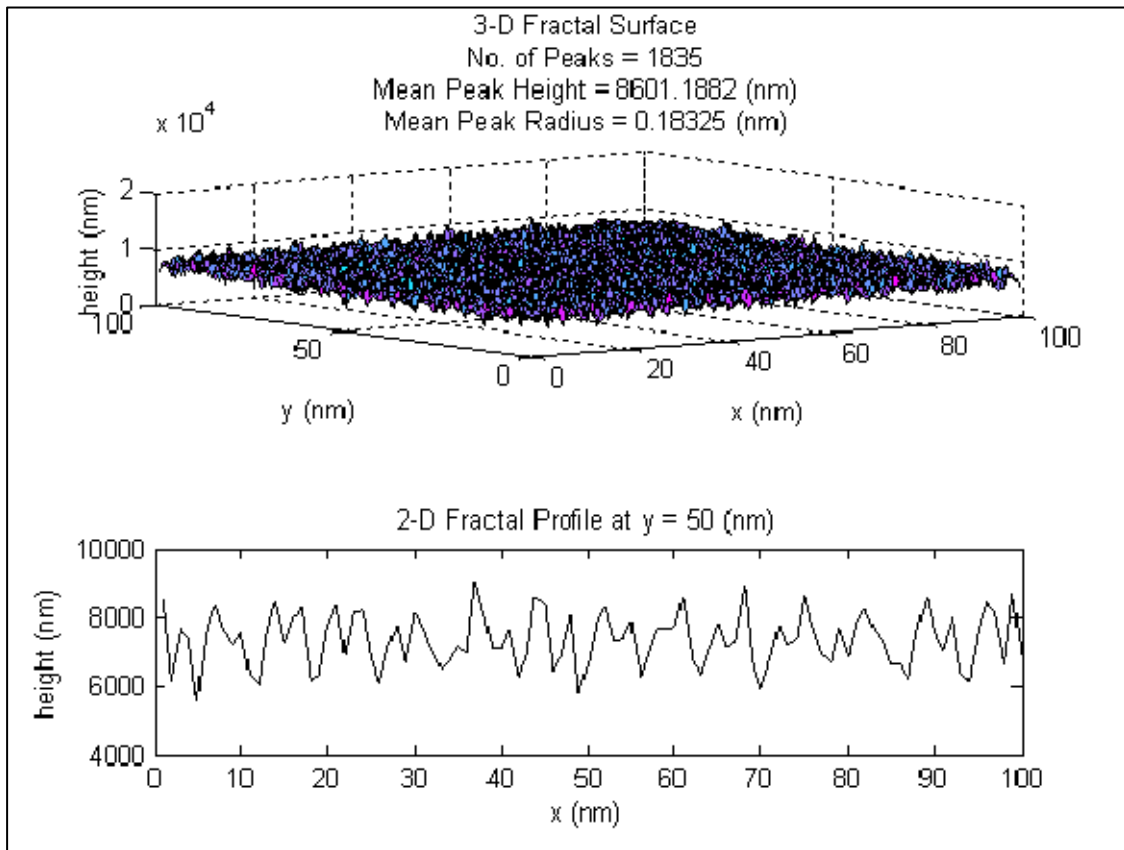


Figure 3. Fractal Surface; Increased M .

When the parameter M was decreased from the baseline value of 10 to 8, the equation yielded a surface and profile as shown in Figure 4. The decreased M resulted again in an increased total number of peaks from 1775 to 1822. The mean peak height decreased, from approximately 7697 to 6794. Similarly, the mean peak radius decreased from 0.59 to 0.19 nanometers. Thus the peaks on average have decreased height and decreased radius, giving lower, narrower peaks.

Although the three-dimensional surface profiles appear similar to the baseline, the two-dimensional profiles display the significant changes when the parameter M is changed. Increased values of M tend to reduce the difference between the peaks and valleys of the figure, causing the frequency band to become narrower. Surprisingly, a decreased value of M also caused some narrowing of the frequency band. The value of M was chosen as the baseline arbitrarily in order to generate a surface profile similar to one shown by Yan and Komvopoulos [5]. Because the equation was designed around the value of M equal to 10, its results yield a profile with the best distribution throughout a large frequency band.

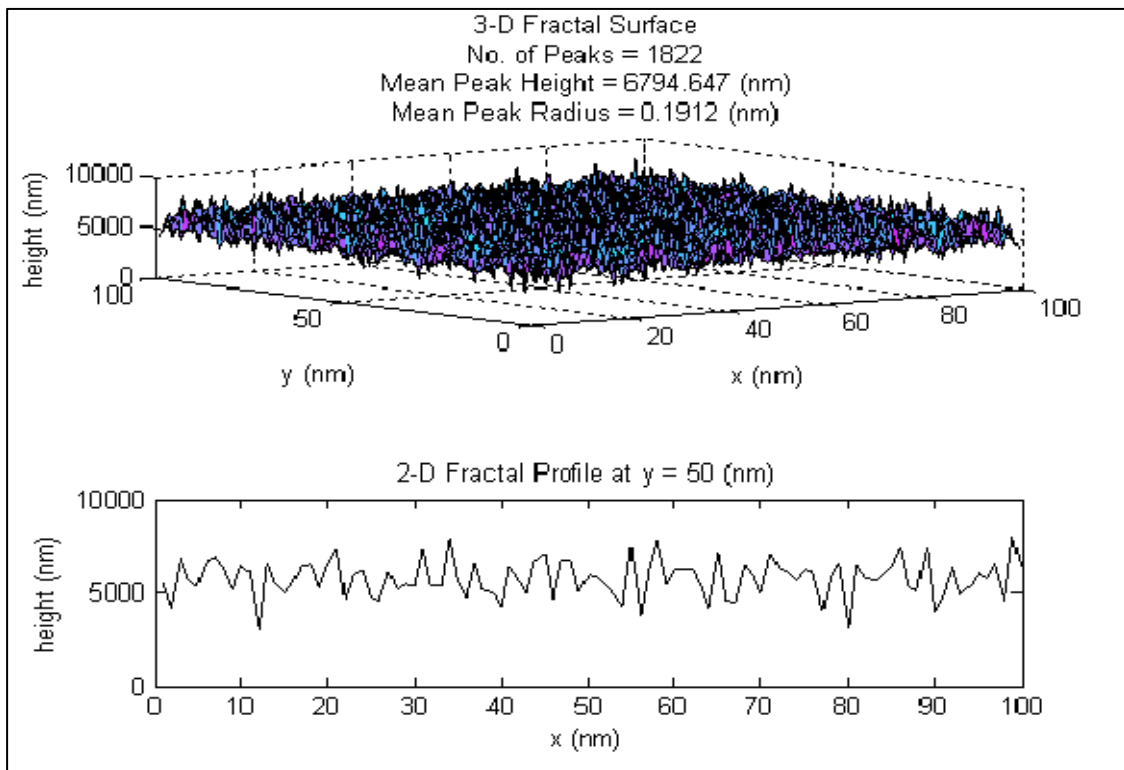


Figure 4. Fractal Surface; Decreased M .

2. Variation of the Fractal Roughness, G

The parameter G in the equation for z in terms of fractal notation represents a height scaling parameter. As it falls outside the summations and trigonometric functions in the equation, it is independent of frequency, and affects the results as a mere scale factor. It is termed the fractal roughness by Yan and Komvopoulos [5]. Increasing the

fractal roughness from the baseline 1.36×10^{-11} to 1.8×10^{-10} meters simply shifts the surface and profile closer to the $x - y$ plane. The overall number of peaks stays the same at 1775, but the mean peak height decreases from 7697 to 975 nanometers. Conversely, because the peak height is changing, it has an effect on the way that the peak radius is calculated. Thus, the mean peak radius increased from 0.59 to 4.69 nanometers, yielding shorter, wider peaks. The results of the increased value for fractal roughness are shown in Figure 5.

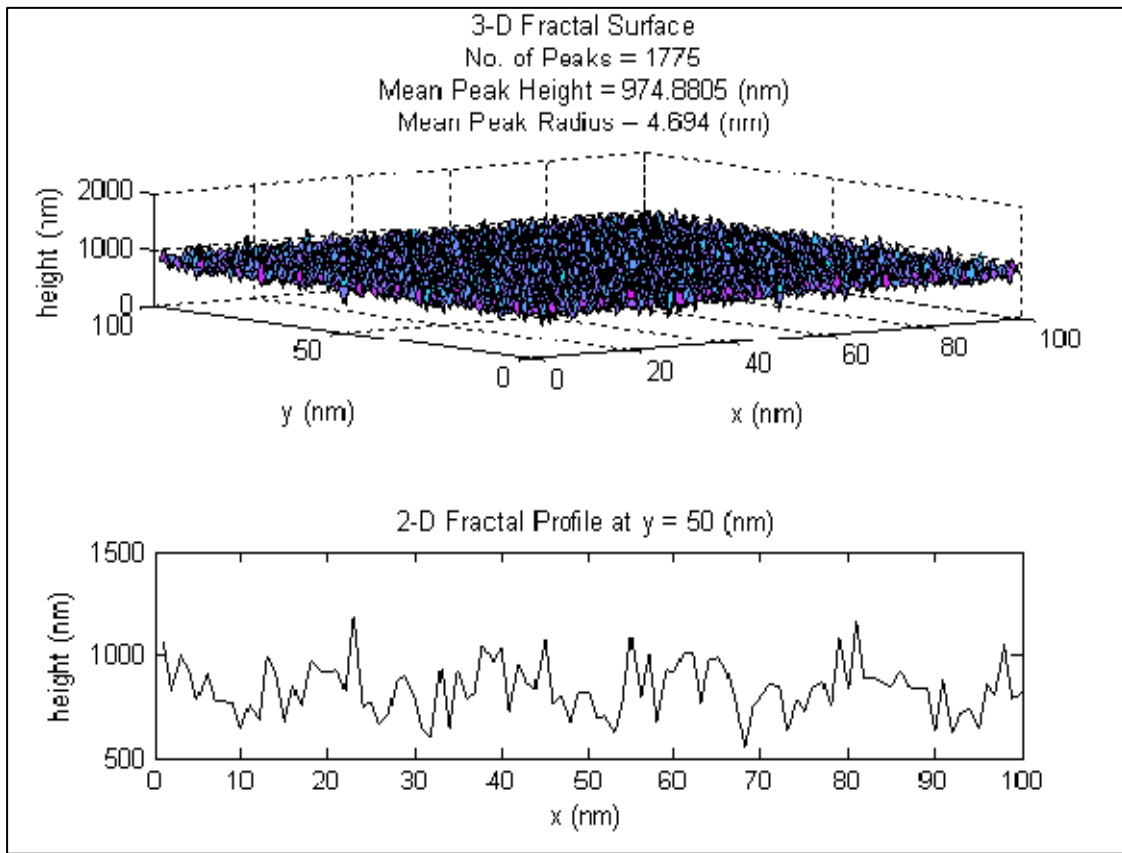


Figure 5. Fractal Surface; Increased G .

Decreasing the fractal roughness from the baseline 1.36×10^{-11} to 3.0×10^{-12} meters simply shifts the surface and profile further away from the $x - y$ plane. The overall number of peaks stays the same at 1775, but this time the mean peak height significantly increases from 7697 to 25791 nanometers. In addition, due to the

significant change in peak height, the mean peak radius decreased from 0.59 to 0.17 nanometers, yielding shorter, wider peaks. The results of the decreased value for fractal roughness are shown in Figure 6.

The parameter G , though it has an effect on the presentation of the surface profile, simply is just a scale factor. It keeps the same peak location, but varies the height and radius at that specific location. G is termed the fractal roughness because as it is increased, it creates lower, smoother peaks. The smoothness of the surface in this case, is the increased peak radius. The larger the peak radius, the greater surface area at the top of the peak; and thus an overall smoother appearance.

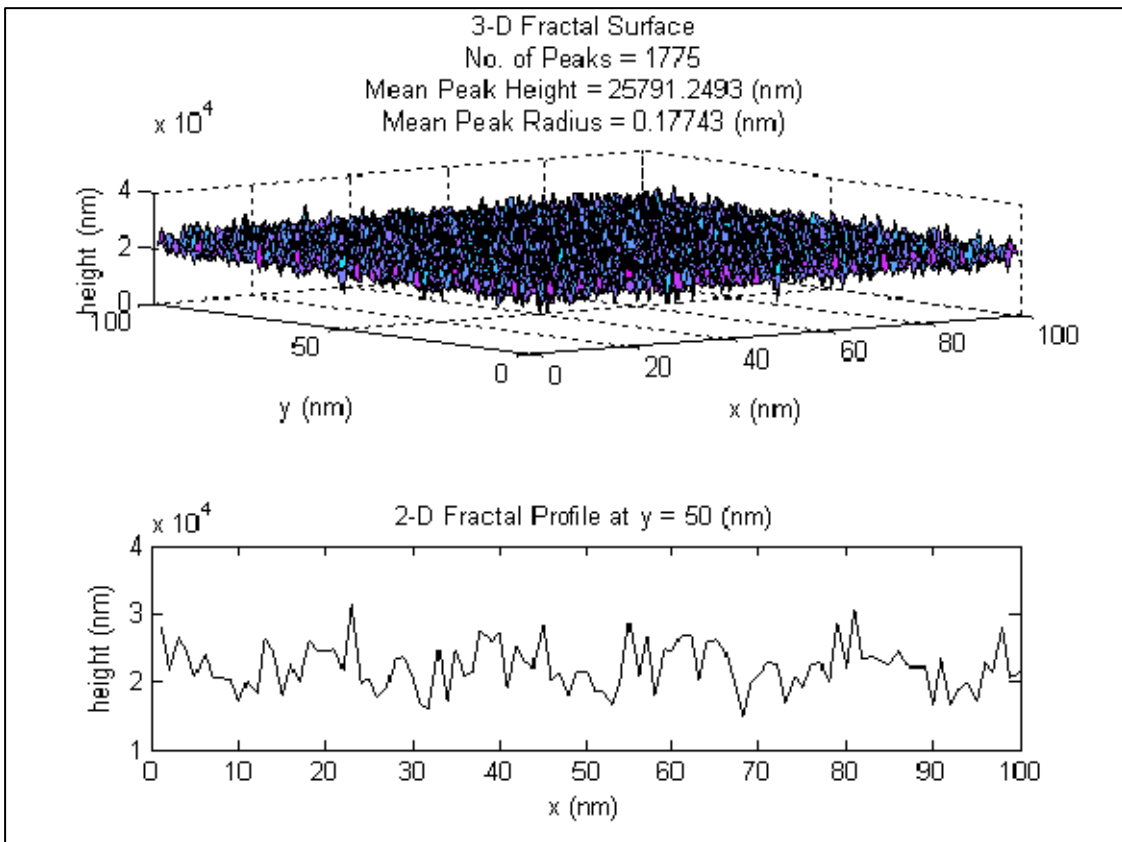


Figure 6. Fractal Surface; Decreased G .

3. Variation of the Fractal Dimension, D

The parameter D in the equation for z in terms of fractal notation represents the fractal dimension. Increasing the fractal dimension from the baseline 1.20 to 1.25

slightly increases the number of peaks from 1775 to 1780. The increased D decreases the mean peak height, however, from 7697 to 5640 nanometers. Conversely, it increases the mean peak radius from 0.59 to 0.87 nanometers. As D is increased, the topography is somewhat smoother, with a narrower frequency band and larger peak radii. Figure 7 shows the new profile with D increased.

When the fractal dimension is decreased from baseline 1.20 to 1.15, it has an opposite effect on the topography, yielding a much more jagged profile. The decreased D develops a mean peak height of 10510 nanometers, more than 2800 nanometers over the baseline. In this case the peak radius decreases from 0.59 to 0.39 nanometers.

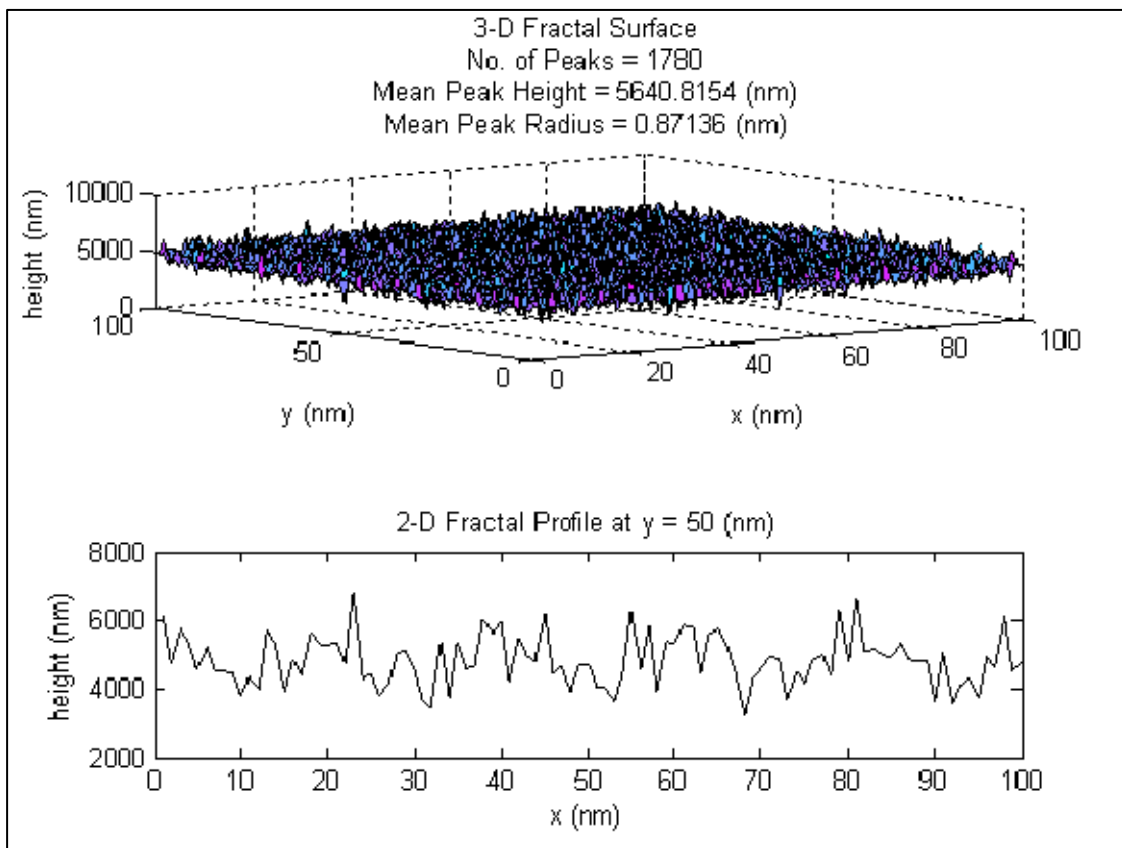


Figure 7. Fractal Surface; Increased D .

The variation of the fractal dimension, D , is a simple way to change the overall surface smoothness. By increasing D , the equation yields a smoother topography, with a narrower frequency band. Decreasing D has the opposite effect. The variation in fractal

dimension has little effect on the actual surface profile shape. The two dimensional profile remains nearly the same for the change in D . Specifically, the shape differences between the profile of the increased and decreased D values is negligible. Scale aside, the profiles are exactly the same. As shown in Figure 8, peak heights are in the same relative location and the overall number of peaks is roughly the same.

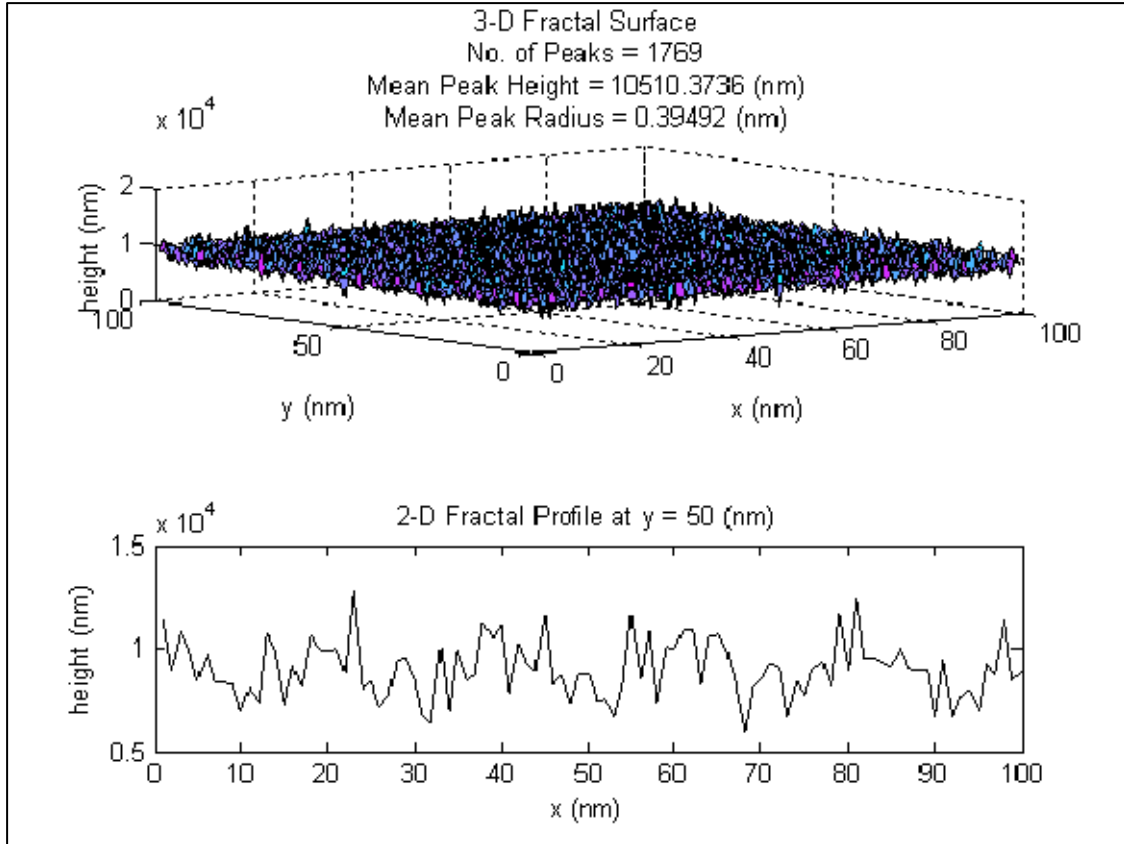


Figure 8. Fractal Surface; Decreased D

4. Variation of the Density of the Profile Frequency, γ

The parameter γ in the equation for z in terms of fractal notation represents the density of the profile frequency. Increasing the density of the profile frequency from the baseline 1.5 to 1.9 has no effect on the number of peaks which remains constant at 1775. The increased γ very slightly decreases the mean peak height, however, from 7697 to 7448 nanometers. It decreases the mean peak radius from 0.59 to 0.23 nanometers. As γ is increased, the topography is somewhat smoother, with a narrower frequency band.

The peak height distribution is more consistent than in the baseline, meaning that many of the tall narrow peaks from the baseline have been replaced with shorter, narrower peaks when γ is increased. Figure 9 shows the new profile with γ increased.

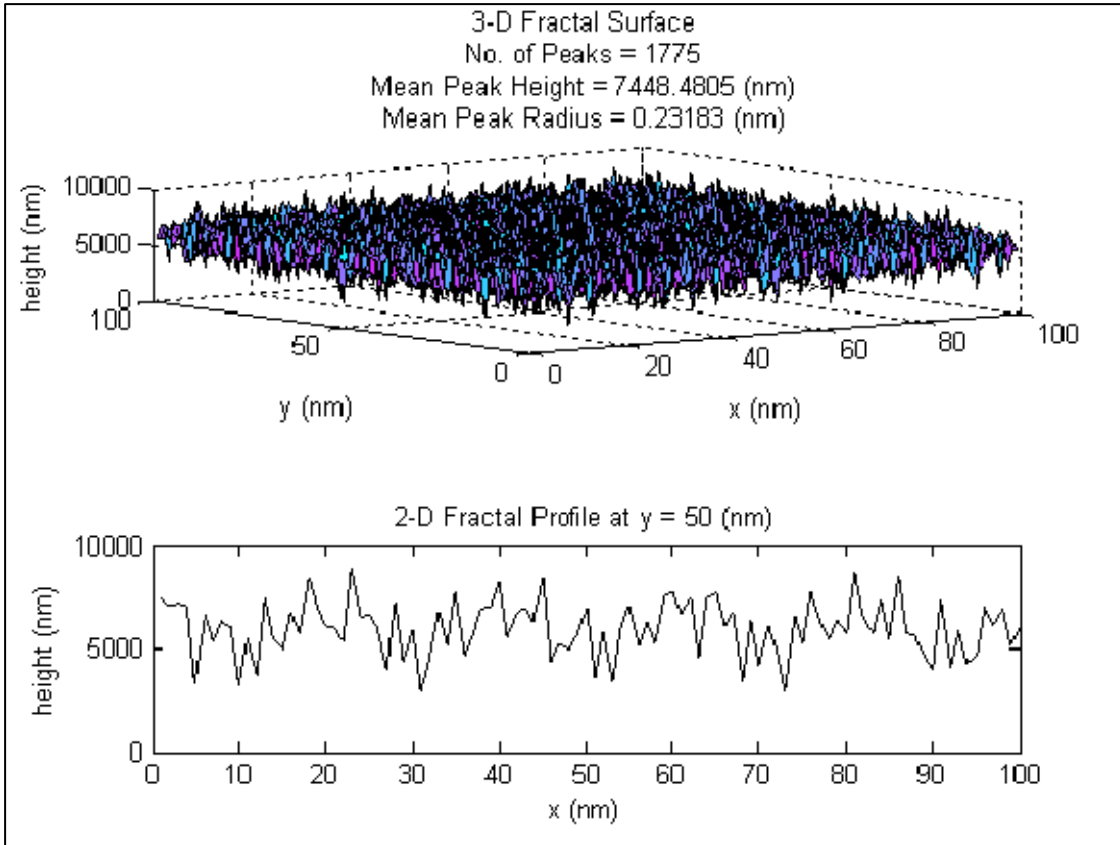


Figure 9. Fractal Surface; Increased γ .

When the density of the profile frequency is decreased, it has a greater effect on the profile. The number of peaks is decreased from 1775 to 1667. Decreasing the density of the frequency, however, causes the mean peak height to increase from 7697 to 8520 nanometers and decrease the mean peak radius from 0.59 to 0.16 nanometers. Thus, the profile is shifted further from the axis, while at the same time the frequency band is decreased when compared to baseline. The surface, with increased profile frequency, is shown as Figure 10.

Yan and Komvopoulos chose the value of γ equal to 1.5 for their studies based upon prior research. They claim that this is the best value for the equation due to

considerations of surface flatness and frequency distribution density [5]. When compared to the increased and decreased γ values, the baseline profile shows the most randomness and variation throughout the profile.

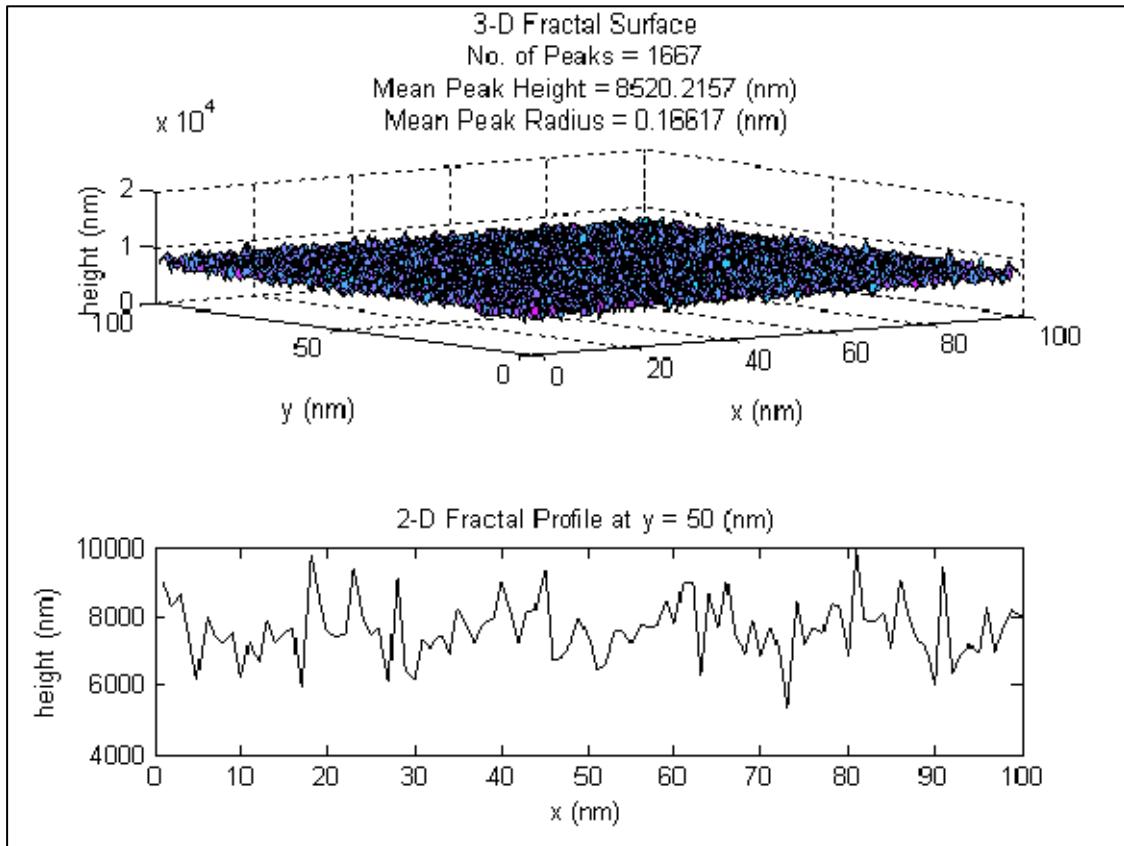


Figure 10. Fractal Surface; Decreased γ .

THIS PAGE INTENTIONALLY LEFT BLANK

III. CONTACT MODELING

A. FORCE-DEFLECTION MODELING

To properly understand the situation of contact, the problem was simplified so that simple Hertz theory could be applied. In order to apply Hertz theory, some assumptions were made in the solutions of the contact problem:

- The contacting bodies are isotropic and elastic.
- The contact areas are essentially flat and small relative to the radii of curvature of the undeformed bodies in the vicinity of the interface
- The contacting bodies are perfectly smooth, and therefore only normal pressures need to be taken into account [2].

Taking into account these assumptions, well-known analytical Hertz equations were used to model each surface peak as a perfect sphere in contact with a rigid flat plate. This assumption required the development of a computer program to solve for each of the thousands of peaks in an extremely small cross-sectional area.

1. Hertz Equations

The simplest form of the Hertz problem is one that describes two spherical surfaces in contact. The contact area in this case is a perfect circle and is described as having a radius, a , as follows [2]:

$$a = 0.88 \left[\frac{P(E_1 + E_2)r_1r_2}{E_1E_2(r_1 + r_2)} \right]^{1/3} \quad (4)$$

The maximum contact pressure, σ_c , is described as:

$$\sigma_c = 1.5 \frac{P}{\pi a^2} \quad (5)$$

Also described is the relative displacement, δ , of the centers of the two spheres due to local deformation and contact at the interface as shown below:

$$\delta = 0.77 \left[P^2 \left(\frac{1}{E_1} + \frac{1}{E_2} \right)^2 \left(\frac{1}{r_1} + \frac{1}{r_2} \right) \right]^{1/3} \quad (6)$$

When the aforementioned equations are again simplified to represent a sphere in contact with a rigid flat plate, the following substitutions are made:

$$\begin{aligned} E_1 &= E_2 = E \\ r_1 &= r \\ r_2 &= \infty \end{aligned} \quad (7)$$

Thus, the equations are simplified as shown below:

$$a = 0.88 \left(\frac{2Pr}{E} \right)^{1/3}, \quad \sigma_c = 0.62 \left(\frac{PE^2}{4r^2} \right)^{1/3}, \quad \delta = 1.54 \left(\frac{P^2}{2E^2r} \right)^{1/3} \quad (8)$$

For this analysis, however, the requirement to impose a deflection and measure the force required to cause that deflection was desired. Therefore, the deflection equation above was solved for the force, P , giving:

$$P = 0.74 |E| (\delta r^{1/3})^{3/2} \quad (9)$$

Using the above equation for the radius, a , of the contact circle, the individual contact area for each sphere against a flat plate was solved as follows:

$$A = \pi a^2 \quad A = \pi \left[0.88 \left(\frac{2Pr}{E} \right)^{1/3} \right]^2$$

Using this equation and the MATLAB program, a force-deflection analysis was completed.

2. MATLAB Program

The simplicity of the Hertz theory allows the development of an analytical solution to be relatively straight forward. Using a complex surface generated by the fractal equation described in the previous chapter, the program analyzes a specific area and identifies the peaks. The peaks are searched for in both the x and y directions individually and are tabulated in a column vector based upon their respective coordinate value. Each time a peak is found, a number is added to the counter, which displays the total number of peaks in a given sample area.

At each of these locations deemed a peak, the height is recorded as the value in the z direction of the standard Cartesian coordinate system. A similar column vector is created to tabulate the local radius of curvature in the x and y directions respectively. These radii of curvature of each peak are averaged as a single radius of a sphere for simplicity. In order to use Hertz theory in the simplified single sphere on a flat plate, the peaks are analyzed individually and treated as local spheres with radii equal to the respective radius of curvature.

The force required to induce (or resist) a given deflection was the desired goal of the program. To achieve this, the relative deflection needed to be solved at each of the peaks. But, since the overall surface had multiple peaks with multiple heights and different radii, a loop needed to be created to separate rigid body motion from contact deflection.

The separation between the fractal surface and the rigid flat plate was defined as the difference in height between each individual peak and the highest peak on the surface. To clarify, if a rigid flat plate was suspended above the surface with no contact, no force would be required. This would be the case as the plate was lowered until it made contact with the highest peak. From this point on, an opposition force would be generated as the plate was lowered and more and more peaks came in contact. Thus, the highest peak was chosen as the reference for the separation data.

To create a force-deflection plot over a span of increasing deflection, a loop was generated to step-increase the deflection from zero to an arbitrary maximum. Simply stated, the program simulated the action of pushing a rigid flat plate onto the peaks of the fractal surface, all the while remaining parallel to the $x - y$ plane. To account for the different peak heights, the separation was used to determine when a specific peak would come into contact with the rigid flat plane. Some of the shorter peaks would never come into contact with the rigid plane, and thus were discounted. The program included a counter to determine the number of effective peaks; the number of peaks that actually were affected by the contact with the rigid plane.

Based upon the separation, contact, and changing relative deflection, calculations were completed at each individual effective peak. The opposition force at each peak was tabulated in a column vector and then summed to determine the overall effective force of opposition through the use of a loop. The summation data was tabulated in a column vector based upon each step decrease of δ , so that the force-deflection data could be plotted. Additionally, using the equation for the contact area of each peak, the program determined the overall effective contact area for each step of δ . Using the data from the force and area calculations, a local contact pressure was solved at each peak and tabulated in a column vector to calculate the overall opposition pressure as the deflection was changed.

The program described above was then slightly modified to include an extra loop that allowed the user to change some of the parameters of the fractal equation and plot the changes. This visual display of the different parametric changes helped to discover some direct relationships between surface profile shape and the changes in effective contact area and opposition force. In all the following figures, the zero displacement starts from the highest peak of the fractal surface.

3. Results, Deflection-Generated Opposition Pressure

Using the aforementioned MATLAB program, plots of the deflection-generated opposition pressure were created to determine the effects of each individual parameter. The figures on the following pages show the results when different parameters are increased and decreased from the baseline.

a. Variation of the Number of Superposed Fractal Ridges, M

As previously discussed in the parametric study, the number of superposed fractal ridges, M , has a significance on the shape of the fractal surface. An increase in M caused an average increase in peak height, and a decrease in peak radius. The expected effect on the deflection-generated opposition pressure matched the results as shown in Figure 11. Increasing the number of superposed fractal ridges caused a significant increase in opposition pressure. This increase is believed to have come from

an increased number of peaks, thus more peaks in contact. More peaks in contact resulted in a greater pressure distribution. Of note, however, is that along with the effect of the wider frequency band of the increased M , the larger deflections have a much greater effect on the contact pressure.

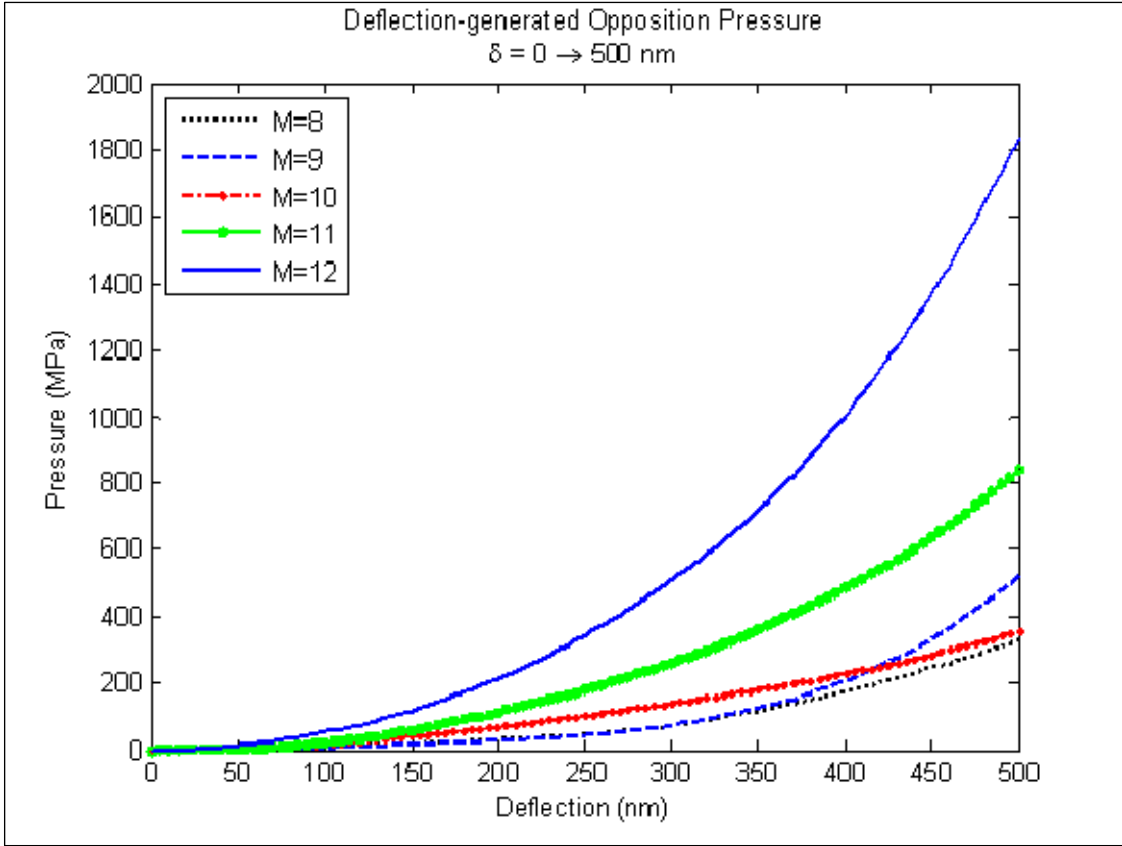


Figure 11. Pressure-Deflection Curves, Changing Parameter M .

The taller peaks make contact first, but as the deflection is increased in steps, the pressure increases as more and more peaks become in contact. The slope of the pressure-deflection curve is much steeper for the case of the increased M .

Conversely, when M is decreased, the effect on the fractal surface is one which decreases the frequency band, peak height, and peak radius. The decreased width of the frequency band has the most significant effect. Because many of the peaks are shorter and closer in height to the surrounding peaks, they all make contact at smaller deflections. Instead of changing rapidly as in the case of the increased M , the slope of

the pressure deflection curve remains much flatter, with very small changes in slope along the length of the curve. The effect of the decrease in M is shown in Figure 11.

b. Variation of the Fractal Roughness, G

The fractal roughness, G , simply represents a height-scaling parameter, and thus the effect of an increase or decrease is directly correlated to the pressure-deflection curve shown in Figure 12.

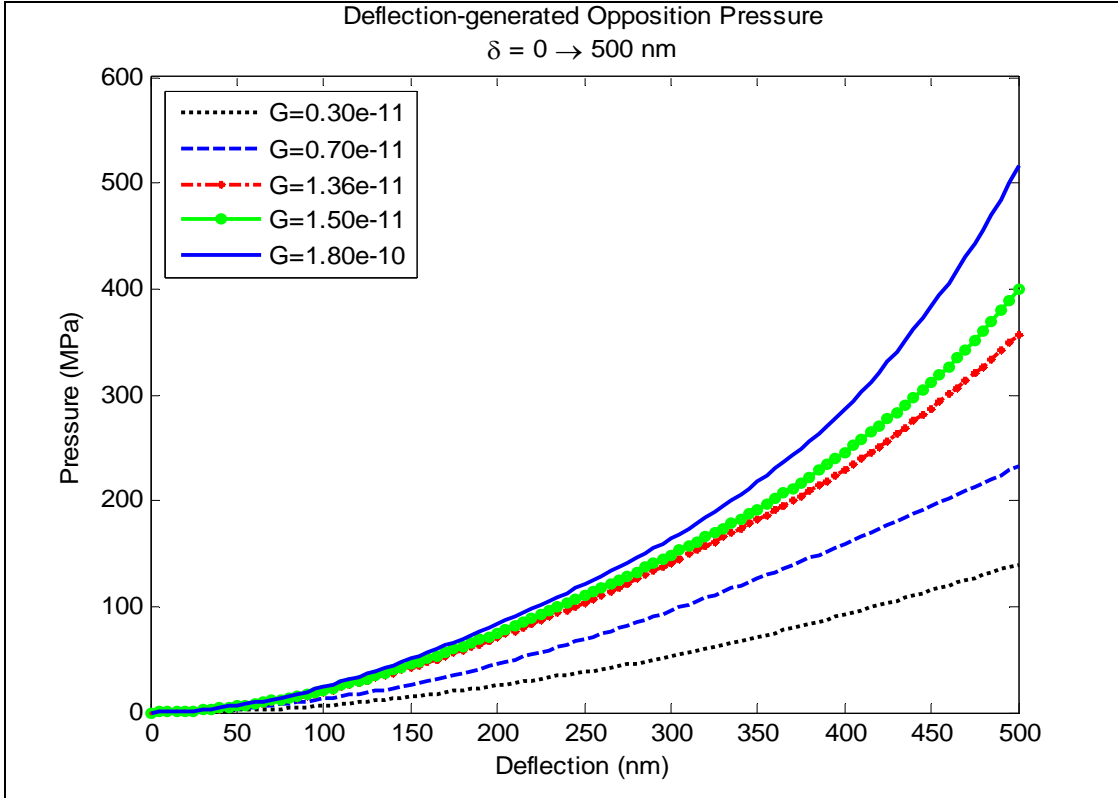


Figure 12. Pressure-Deflection Curves, Changing Parameter G .

The Increasing the fractal roughness shifts the pressure-deflection curve up. The value for the peak radius is calculated based upon a change in peak height in a specific direction, and since an increase in G causes the peaks to become shorter, the radius is directly affected. When G is increased, peak radius increases. Wider, shorter peaks will have a greater contact area and thus greater pressure for the same force.

Conversely, a decrease in G has the opposite effect. Peak heights are significantly increased, but radius is significantly decreased. The taller, narrower peaks make contact in the same manner as the shorter wider peaks, but the decreased radius causes a decrease in contact area. Thus, the contact pressure is decreased, yielding a much flatter pressure-deflection curve as shown in Figure 12.

c. Variation of the Fractal Dimension, D

The fractal dimension, as previously discussed, changes the smoothness of the fractal surface. An increase in D develops a smoother topography with narrower frequency band. In addition, the peak radii are increased, which causes more peak surface to be in contact. The small changes of D are shown in Figure 13. Although the curves are slightly different, they all follow the same trend. As previously discussed, the surface profile shape remains virtually the same for different values of D , the largest change being the peak height. An increase in D caused a decrease in peak height, and a decrease caused a significant increase in height. Thus, the shorter peaks made contact over a larger area, causing a steeper pressure-deflection curve, whereas the taller peaks had the opposite effect.

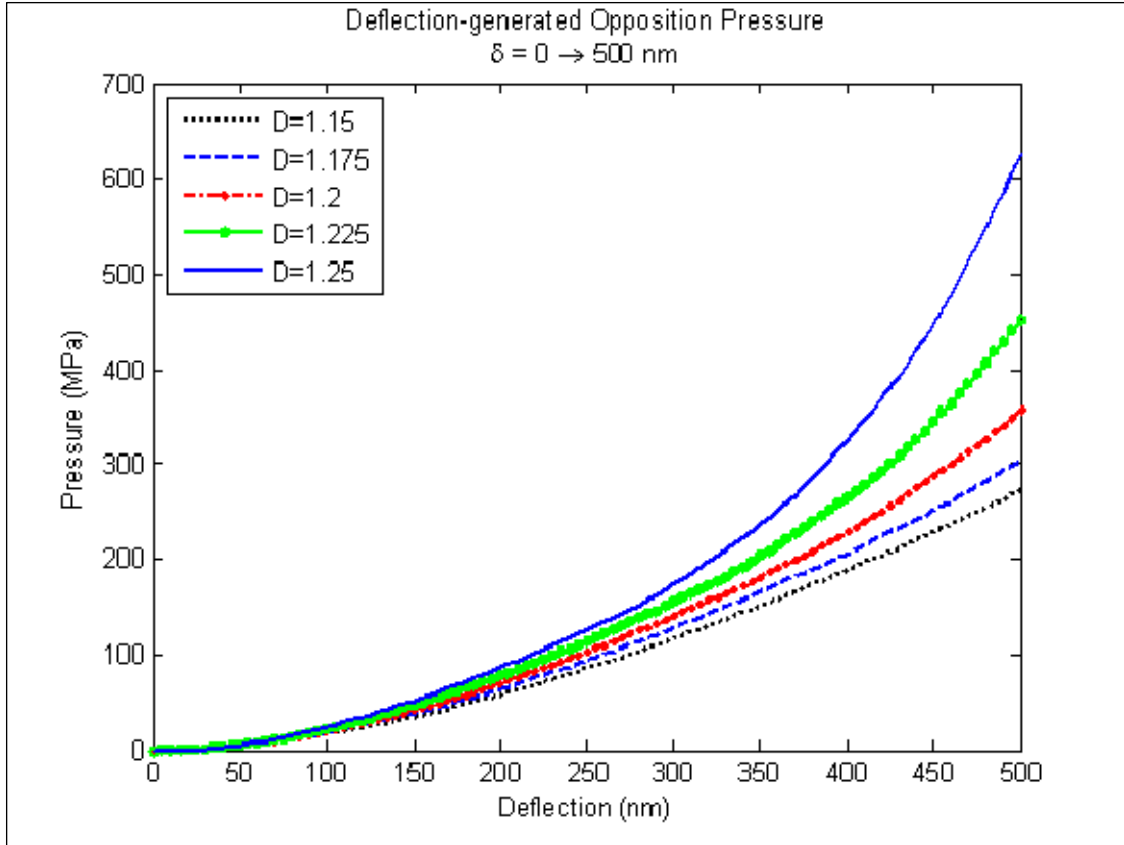


Figure 13. Pressure-Deflection Curves, Changing Parameter D .

d. Variation of the Density of the Profile Frequency, γ

The density of the profile frequency had different effects on the surface topography as was previously discussed. Thus, the profile was inconsistent for different values of γ . Predicting the shape of the profile based on the γ value was inconclusive. Thus, the originators of the fractal surface equation, Yan and Komvopoulos, chose the value equal to the baseline of 1.5 based upon their prior research. The pressure-deflection curves are shown below in Figure 14, but direct correlation to the effects due to the parameter γ was not possible.

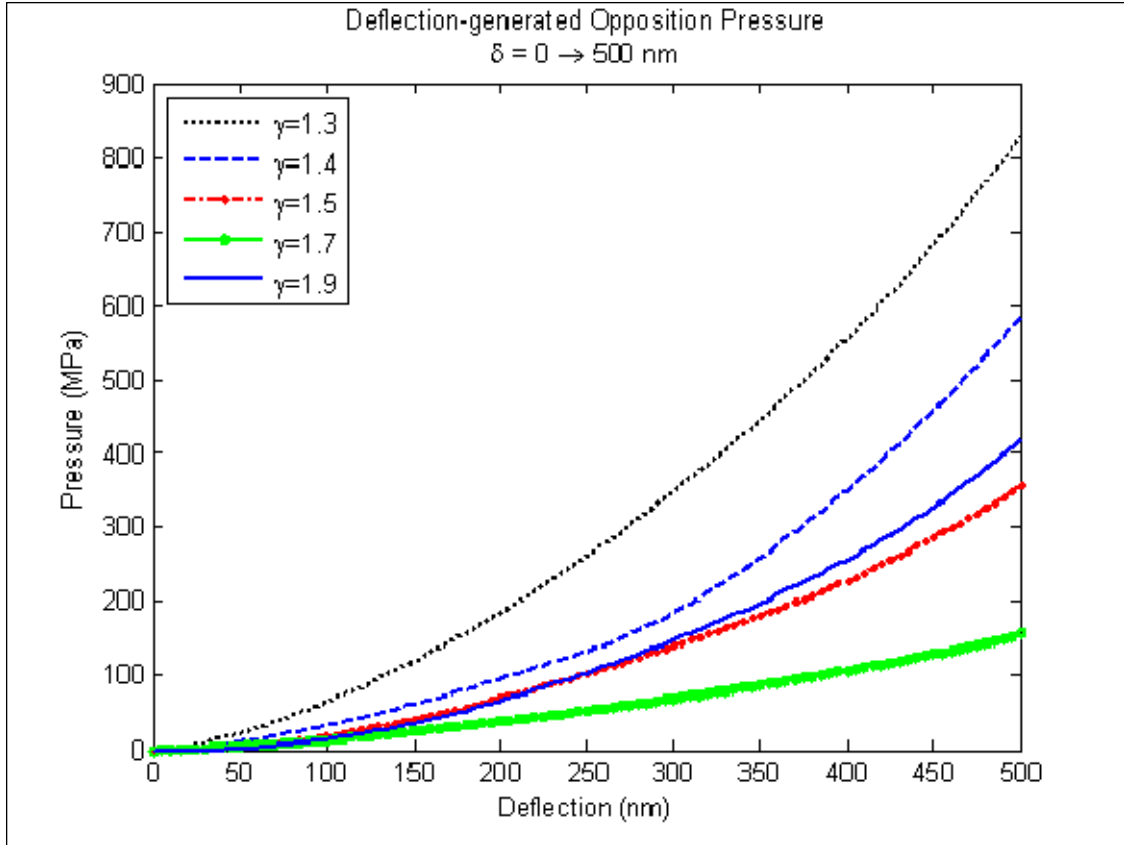


Figure 14. Pressure-Deflection Curves, Changing Parameter γ .

4. Results, Deflection-Generated Contact Area Ratio

a. Variation of the Number of Superposed Fractal Ridges, M

The effect of the various values of M was fairly simple to determine based upon the results of the parametric study previously conducted. Increasing the number of superposed fractal ridges caused increased peak height and decreased radius. Although the initial peak radius had an effect on the contact area, the formulation of the equation to solve for the continued increase in contact radius after a peak made contact caused the actual area to increase significantly. The effect was that the taller peaks, made contact early, and their small peak radii increased at a rate much greater than the baseline. The results are shown below in Figure 15.

Conversely, the decrease in M caused the peaks to become shorter while at the same time having a decreased peak radius. Thus, the peaks came into contact much sooner and the peak radii would all increase at the same time as the other peaks in contact. Therefore, the percentage of area in contact did not significantly change over the range of deflections shown. The results matched what was expected based upon the fractal surface shape and profile.

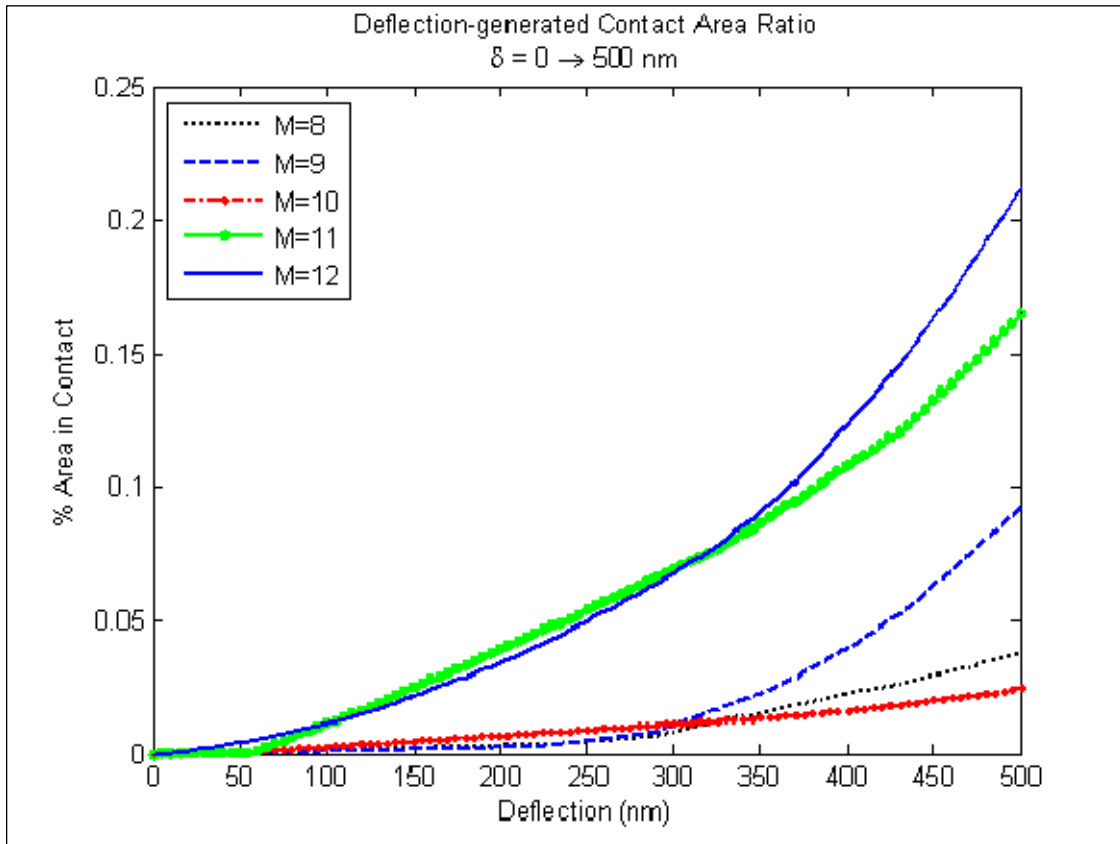


Figure 15. Area Ratio-Deflection Curves, Changing Parameter M .

b. Variation of the Fractal Roughness, G

Similar to the effects upon the pressure-deflection curves, the variation of G had the exact same effect on the area-deflection curve shown below as Figure 16. The decreased G flattened the curve, whereas the increased G caused a steep increase in the curve. Again, the reason for this change in shape is due to the fact that the fractal

roughness simply is a height scaling parameter. The radius was calculated based upon the change in height (or radius of curvature) at the peak, and thus the effect is directly correlated.

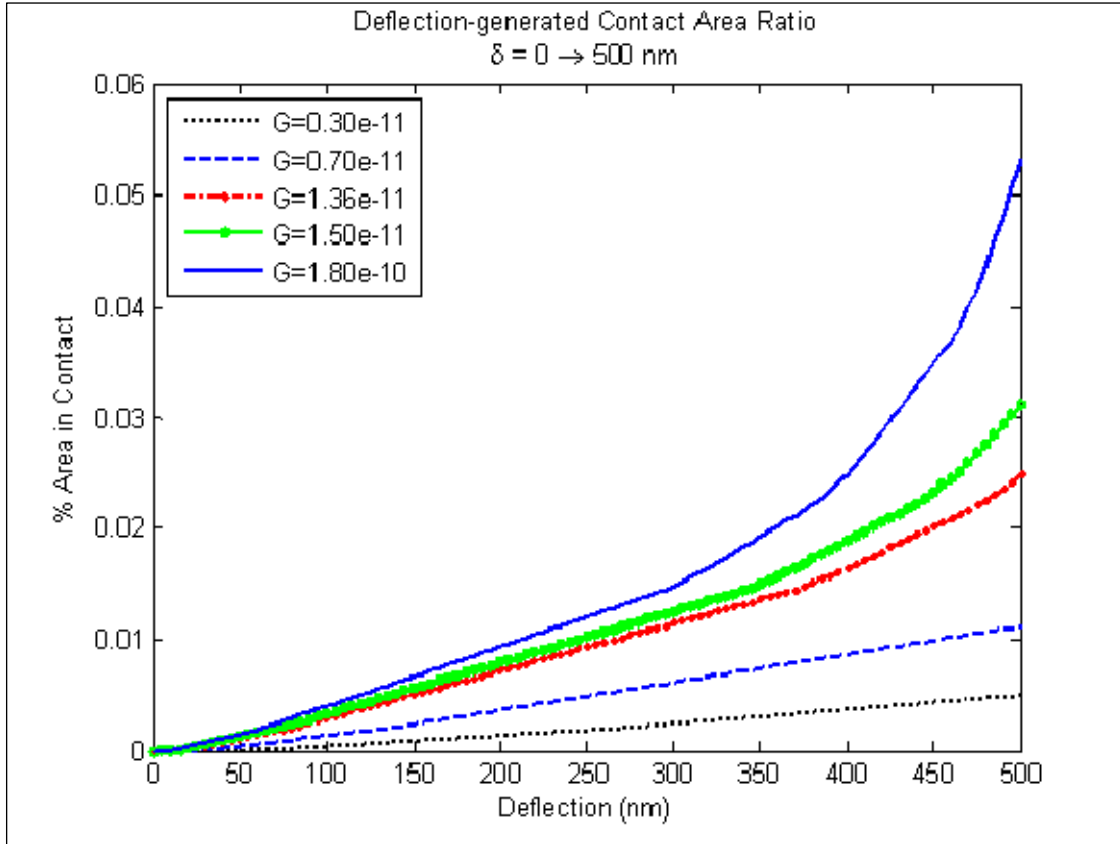


Figure 16. Area Ratio-Deflection Curves, Changing Parameter G .

c. Variation of the Fractal Dimension, D

An increase in D developed a smoother topography with narrower frequency band. The smoother the topography is, the more area is in contact. When D is decreased, the topography becomes more jagged, and thus fewer peaks make contact. The decreased number of peaks in contact causes a decrease in contact area ratio. The results of the variation of fractal dimension are shown below as Figure 17.

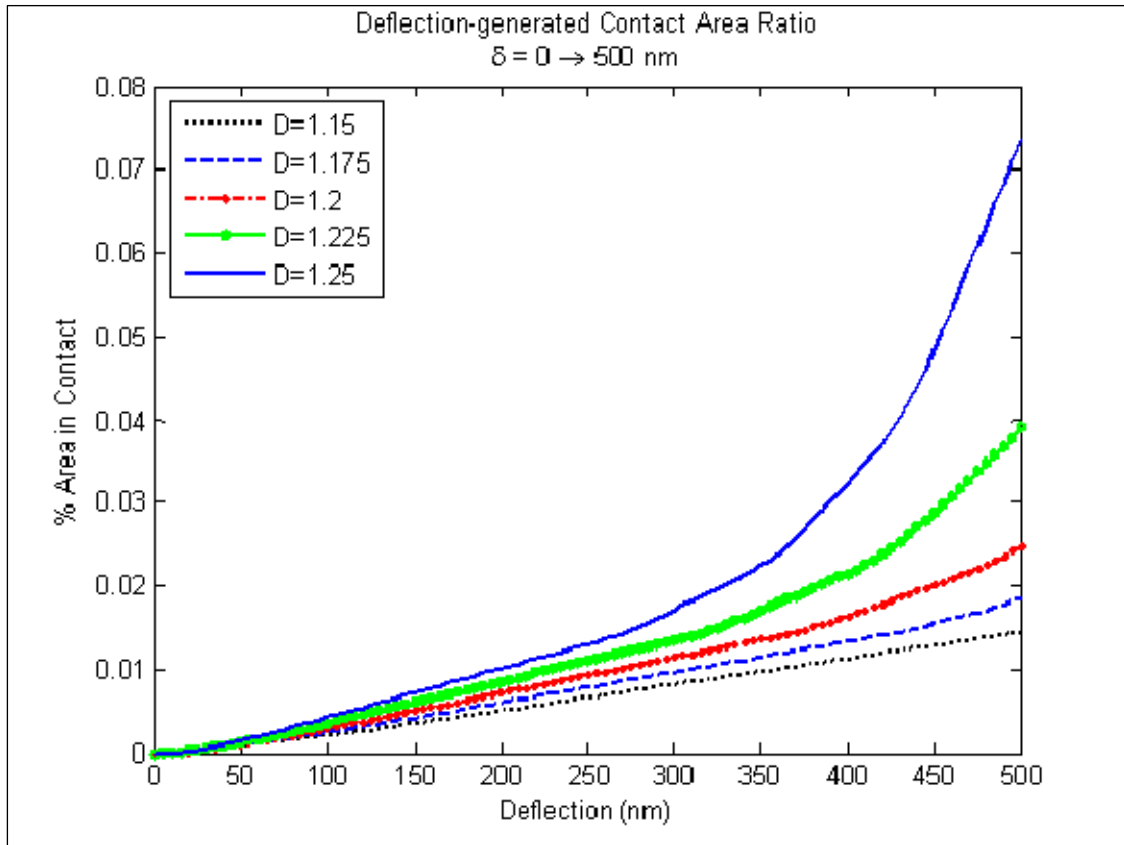


Figure 17. Area Ratio-Deflection Curves, Changing Parameter D .

d. Variation of the Density of the Profile Frequency, γ

Varying the density of the profile frequency, as previously stated, was inconclusive as far as estimation of surface shape and profile was considered. Thus, the effect on contact area ratio was also varied based upon the different profile frequencies. Again, the value of γ equal to 1.2 was chosen by the originators of the equation based upon previous research in surface flatness and frequency distribution. The results of the area-deflection plot are shown below as Figure 18.

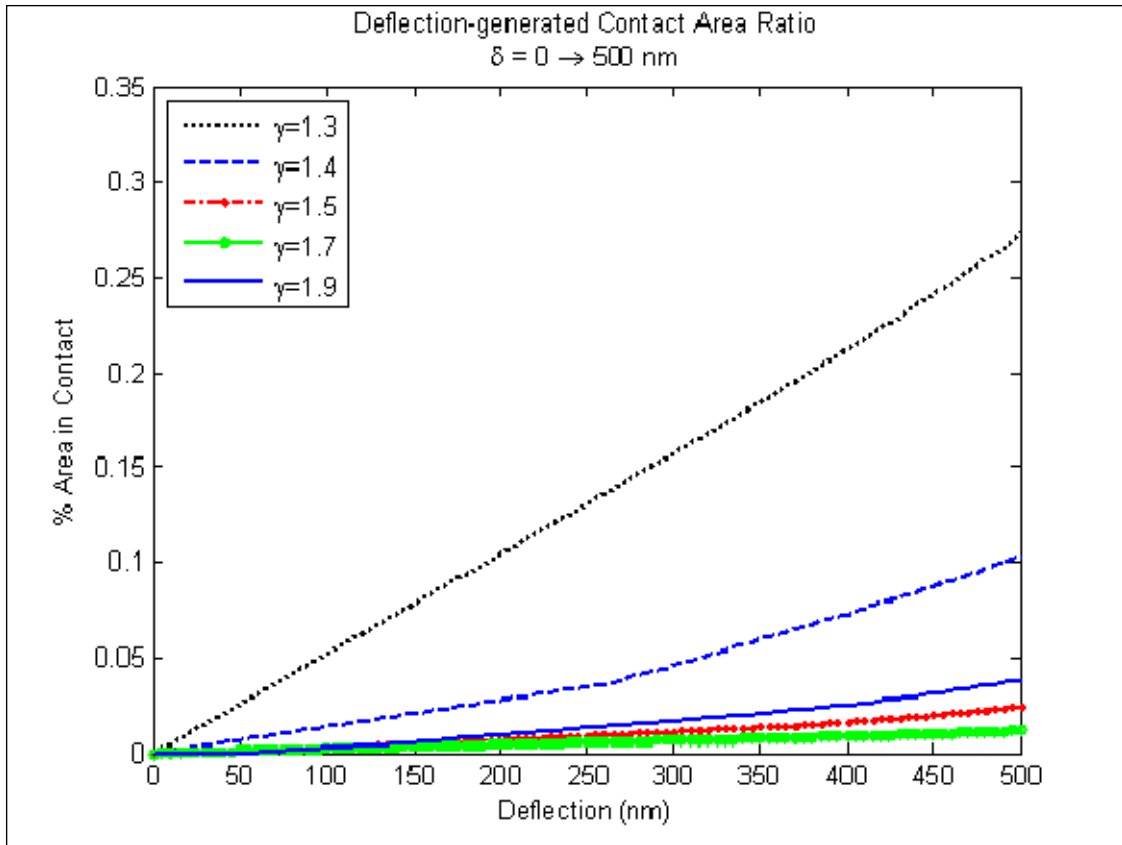


Figure 18. Area Ratio-Deflection Curves, Changing Parameter γ .

5. Curve Fitting

In order to properly analyze the results, it was desired to find suitable equations for the deflection-generated opposition pressure and the area-deflection curves, respectively. Using MATLAB and its embedded code for polynomial curve-fitting, the pressure and area curves were solved using linear, quadratic, and cubic equations. The results of each polynomial fitting were assembled and plotted along with the raw data to determine which equation best fit the data. The goal was to determine an equation that was both simple and accurate, and thus research beyond the level of the cubic polynomial was not considered. The results are shown below as Figure 19. Although the quadratic equation does a reasonably good job of fitting the data, it was determined that the cubic remains closer to the data throughout the range of deflection. These cubic equations were then used in the Railgun program discussed in the next chapter.

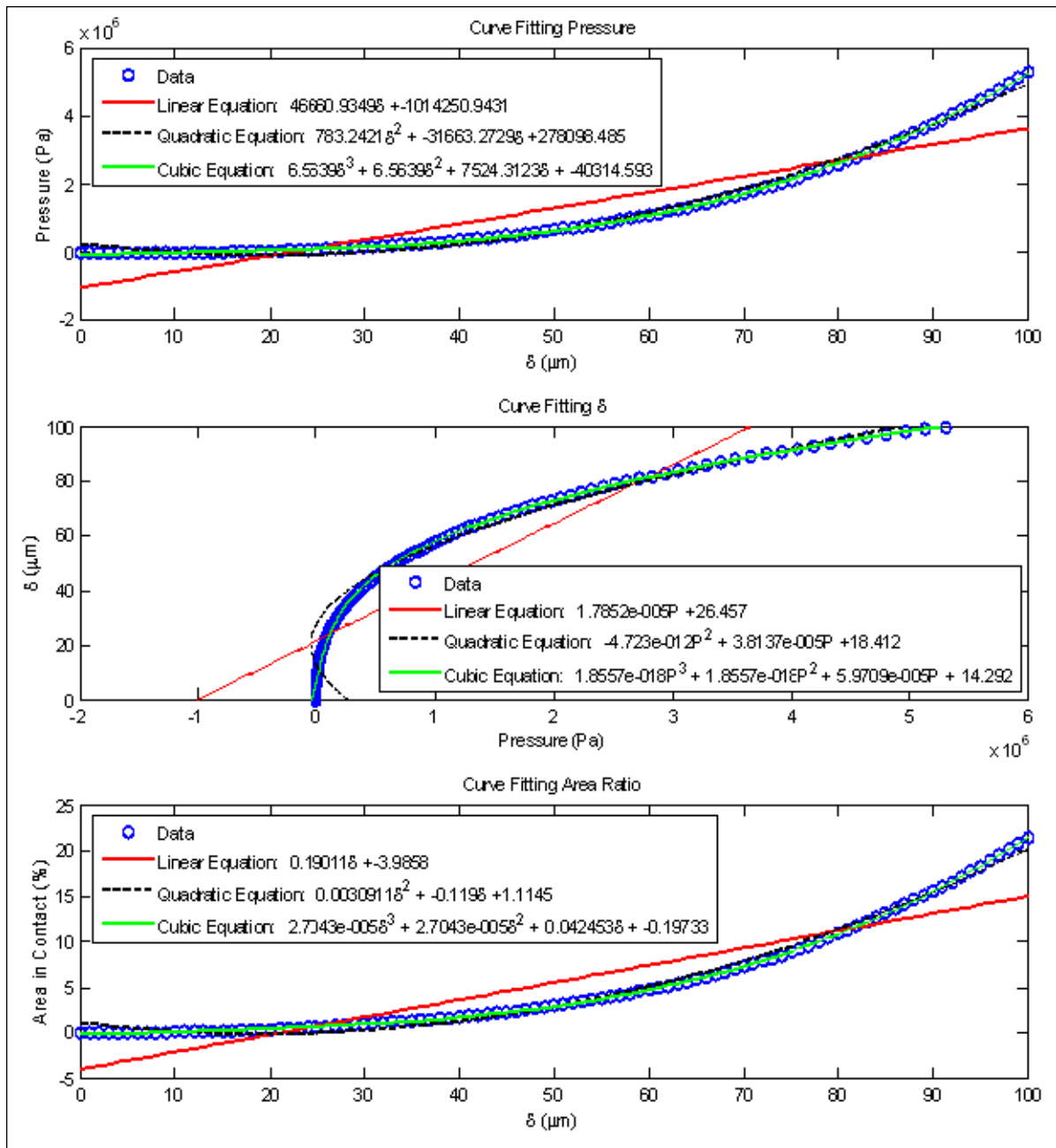


Figure 19. Polynomial Curve-Fitting.

V. RAIL-GUN MODELING AND ANALYSIS

A. INTRODUCTION

The research completed for this thesis focused on the contact problem encountered during the development of the electromagnetic rail gun. A study of the specific interface between the armature and the rails was necessary to properly understand the mechanics in this area. The thesis research of Nikolaos Pratikakis in 2006 focused on the development of a mathematical model of the electromagnetic rail gun. Using the equations developed in the previous chapter, the Pratikakis model was slightly modified to reflect the research of this thesis.

B. PRATIKAKIS MODEL

The mathematical model created by Nikolaos Pratikakis was developed using MATLAB code and the finite element method. It was made up of two main parts which are briefly summarized below.

1. Part I, Setup of Inertial Coordinate System and Geometric Configuration

Part I of the program was the development of the specific geometric dimensions and mesh of the model based upon lengths and widths of the rails and projectile as provided by the manufacturer. The geometry was simplified into a two-dimensional, uniform rectangular mesh for both the rails and the armature. Of note, however, is that the geometry could be changed very simply to account for different shaped armatures [9].

2. Part II, Main Program and Description of Functions

A schematic of the rail gun program is shown as Figure 20. This program completes many calculations during each loop that properly account for the multi-physics nature of rail gun functioning. Specifically, electrical current density and current distribution are used to determine the total heat generated due to electrical resistance. These values are also used to determine the Lorentz Force on the projectile. Using partial differential equations, the program also completes a stress analysis to estimate the x and

y displacements. Thermal stresses are also calculated by assuming that the rails are fixed and rigid. The acceleration of the armature is also calculated using the second law of Newton. The program continues to run in an iterative loop until the displacement of the projectile is larger than the length of the rails, at which it records an exit velocity [9].

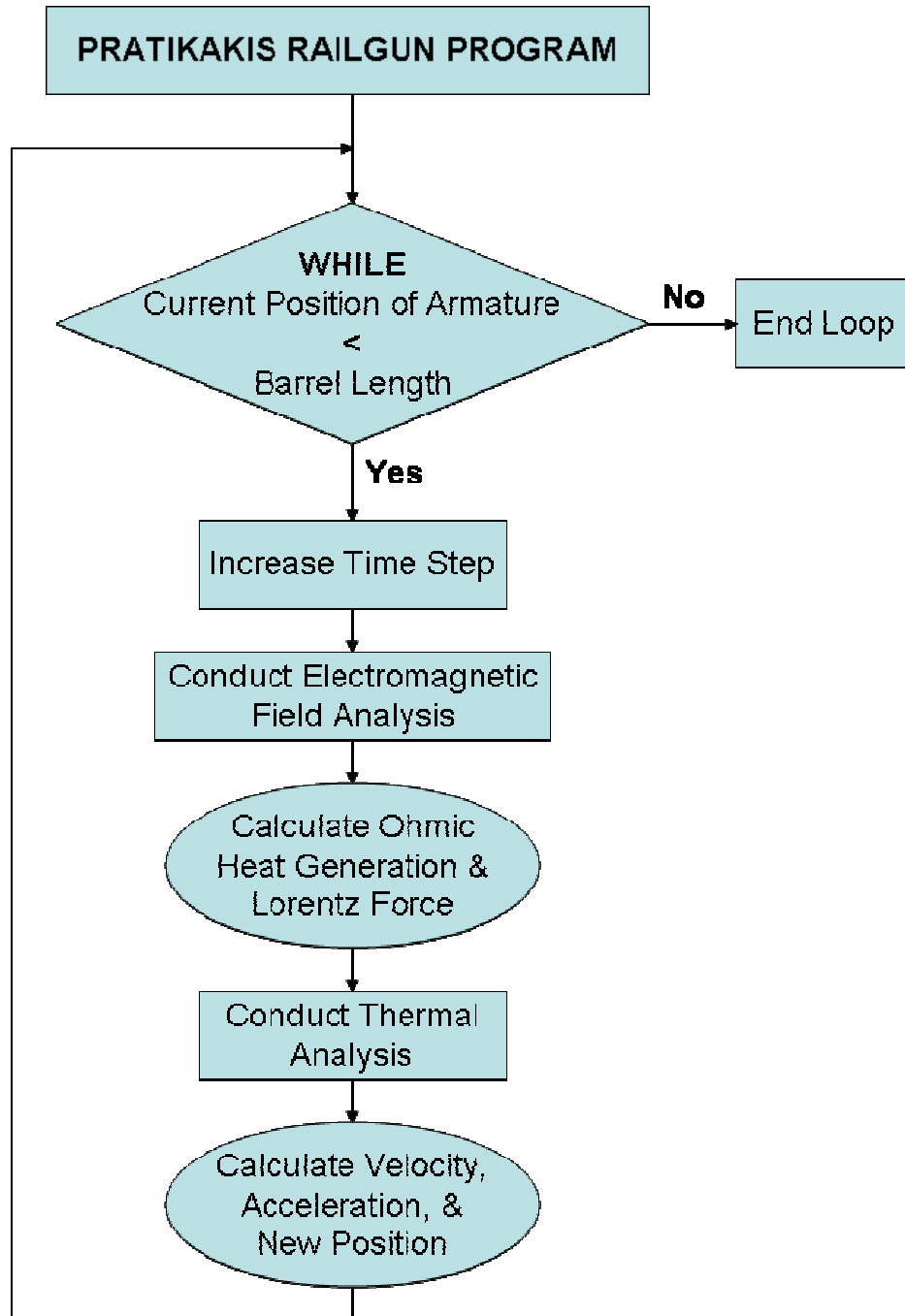


Figure 20. Schematic of Rail Gun Program [8].

C. RESULTS OF MODIFIED PRATIKAKIS EQUATION

In order to properly understand the effects of each of the fractal parameters in a real-world application, the Pratikakis rail gun program was used. Using this program, a baseline set of results was generated using the nominal values previously discussed in this thesis. Then, the following parameters were altered: number of superposed fractal ridges, fractal roughness, fractal dimension, and profile frequency.

1. Variation of the Number of Superposed Fractal Ridges, M

Using 10 as the baseline value of M , the parameter was decreased to the values 8 and 9, and increased to the values 11 and 12. Each time the parameter was changed, the Pratikakis rail gun program generated the values of the area ratio, electrical conductivity, maximum temperature, and velocity of the projectile at the time at which it exits the rails. These results were recorded for each of the four different variations of the parameter, M . In order to gain a better sense of the change, the results were all normalized against the baseline value for comparison. The results of this parametric change are shown as Figure 21 with one exception. When the program was run with a value of M equal to 9, it produced results which were a significant outlier. When the normalized data was plotted, the $M = 9$ data resulted in a plot that was almost impossible to discern the other values of M , and thus this set of results was left out of the figure.

When the number of superposed fractal ridges was decreased or increased, it caused the values for all four of the measured output quantities to increase. As previously discussed, the decrease in M results in shorter, narrower peaks, whereas the increase in M results in taller, narrower peaks. The effect of the narrowing of peak radius may result in a greater contact area, which allows for improved electrical conductivity. The greater the electrical conductivity, the more efficient Lorentz force, which results in a greater exit velocity and higher temperature. Of note in Figure 21 is that all four plots display the same trend on different scales. This is believed to be a trend strongly influenced by the effective area ratio.

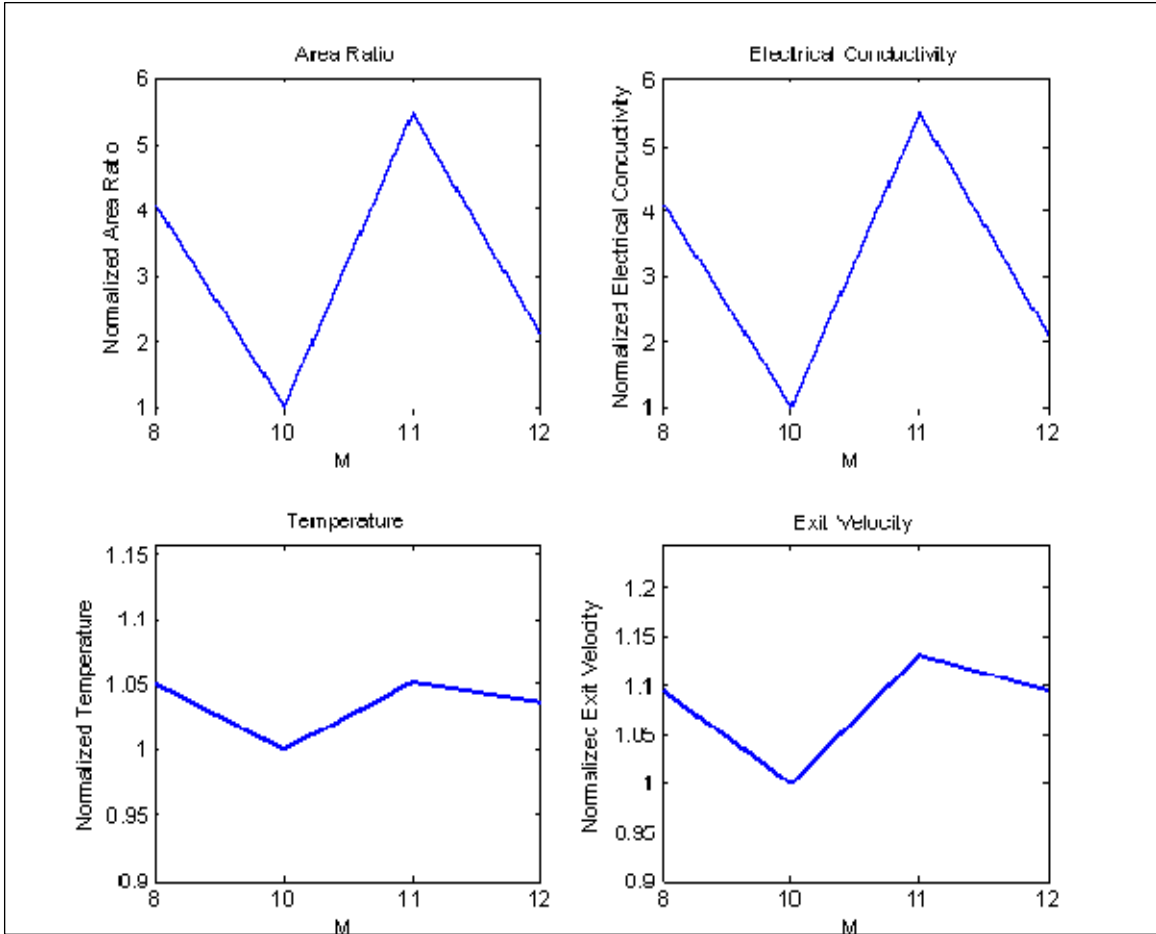


Figure 21. Variation of the Number of Superposed Fractal Ridges, M .

2. Variation of the Fractal Roughness, G

Using 13.6 picometers (1.36×10^{-11} m) as the baseline value of G , the parameter was decreased to the values 0.30×10^{-11} and 0.70×10^{-11} , and increased to the values 1.50×10^{-11} and 1.80×10^{-10} meters. Each time the parameter was changed, the Pratikakis rail gun program generated the values of the area ratio, electrical conductivity, maximum temperature, and velocity of the projectile at the time at which it exits the rails. These results were recorded for each of the four different variations of the parameter, G . In order to gain a better sense of the change, the results were all normalized against the baseline value for comparison. The results of this parametric change are shown in Figure 22.

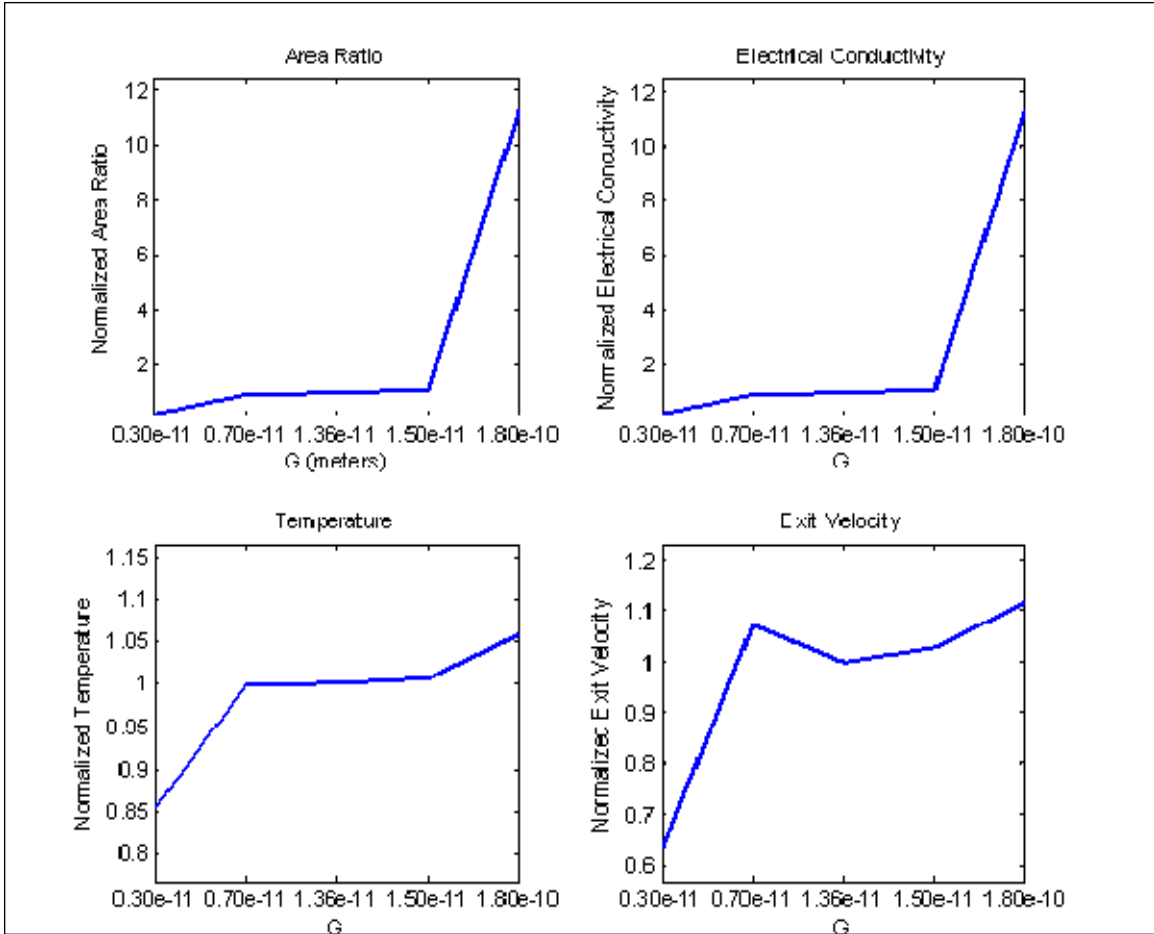


Figure 22. Variation of the Fractal Roughness, G .

When the fractal roughness was decreased the area ratio, electrical conductivity, and temperature all decreased, but the exit velocity increased slightly at $G = 0.70 \times 10^{-11}$ and decreased at $G = 0.30 \times 10^{-11}$. As previously discussed, when the parameter G is decreased, the surface peaks become slightly shorter and wider, but the number of peaks remains the same. The wider peak radii decrease the deflection that occurs at the contact surface, and thus decreases the change in contact area. This, in turn, decreases the conductivity, temperature, and exit velocity. An exception occurs at the value of $G = 0.70 \times 10^{-11}$ meters, where the exit velocity increases when compared to baseline when all of the other parameters have decreased.

When the fractal roughness was increased, the area ratio, electrical conductivity, temperature, and exit velocity all increased. When G is increased, the result is taller, narrower peaks. Again, the effect of decreased peak radius is that the area ratio may change easily as a force is applied. The increased area ratio thus dominates the rest of the results, and yields an increase in electrical conductivity, temperature, and exit velocity. Of note, is when G is significantly increased as is the case when $G = 1.80 \times 10^{-10}$ meters, resulting area ratio increase is immense, and has a direct effect on the other quantities calculated.

3. Variation of the Fractal Dimension, D

Using 1.20 as the baseline value of D , the parameter was decreased to the values 1.15 and 1.175, and increased to the values 1.225 and 1.25. Each time the parameter was changed, the Pratikakis rail gun program generated the values of the area ratio, electrical conductivity, maximum temperature, and velocity of the projectile at the time at which it exits the rails. These results were recorded for each of the four different variations of the parameter, D . In order to gain a better sense of the change, the results were all normalized against the baseline value for comparison. The results of this parametric change are shown as Figure 23.

As was previously discussed, the fractal dimension is the simplest way to change the overall surface smoothness. Increasing D yields a smoother topography with a narrower frequency band. The relative shape of the profile remains unchanged, such that peaks remain in the same location, but their heights and radii may change. Thus, one can expect different results when the frequency band is narrowed. Because the fractal dimension predominantly effects peak height, and in turn, frequency band, the results of the Pratikakis program are difficult to determine based on this parameter alone.

In the case of $D = 1.15$ and $D = 1.25$ all results decrease compared to the baseline, whereas in the other two cases tested, the results increase. The conclusions gathered from this result is that the peak height and frequency band may have counteractive effects on the contact area. In some instances, the peak height may cause fewer peaks to be in contact, but be easily deformable, and in other cases such as a slight

increase, there may be more peaks in contact, but be more difficult to deform. Thus, one must examine the size of the frequency band and the actual profile before trying to determine the direct effects of the variation of the fractal dimension, D .

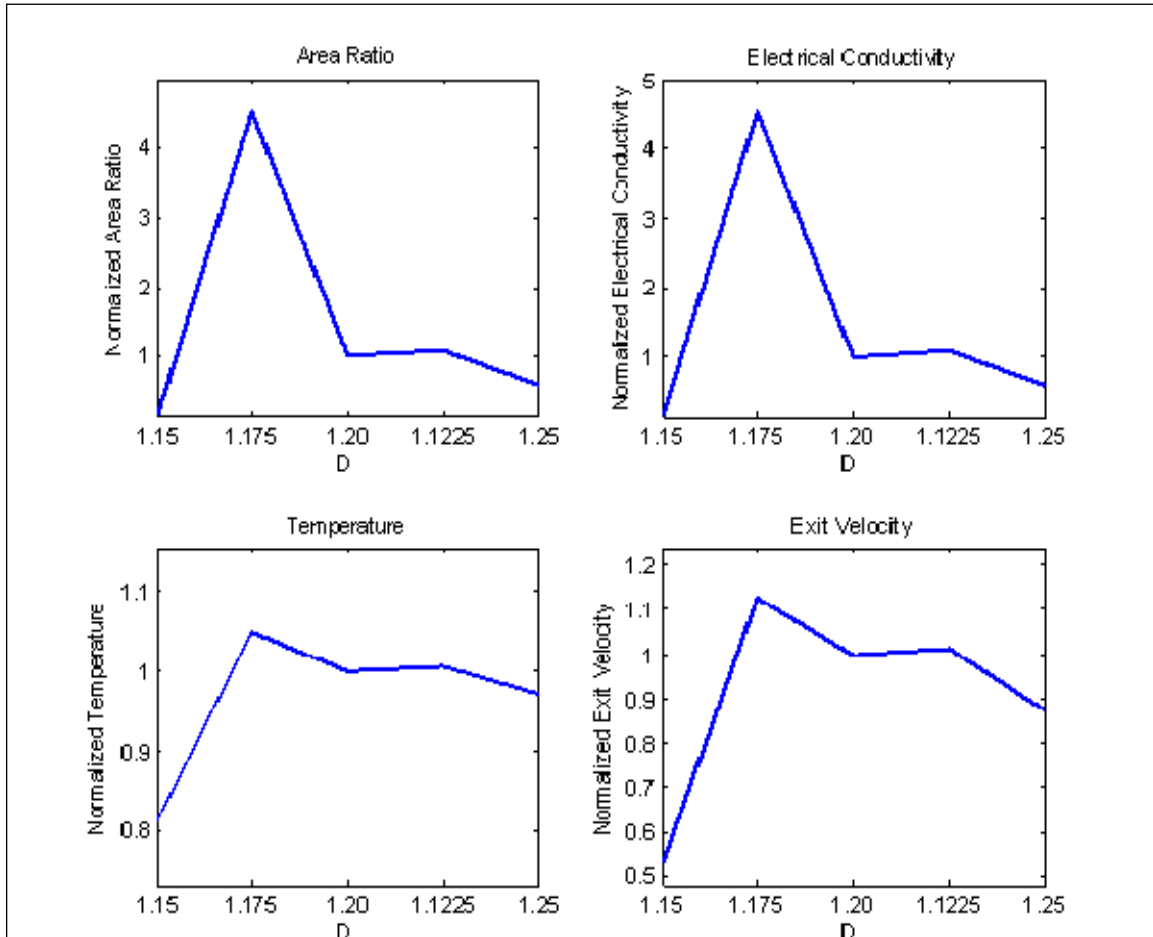


Figure 23. Variation of the Fractal Dimension, D .

4. Variation of the Density of the Profile Frequency, γ

Using 1.5 as the baseline value of γ , the parameter was decreased to the values 1.3 and 1.4, and increased to the values 1.7 and 1.9. Each time the parameter was changed, the Pratikakis rail gun program generated the values of the area ratio, electrical conductivity, maximum temperature, and velocity of the projectile at the time at which it exits the rails. These results were recorded for each of the four different variations of the

parameter, γ . In order to gain a better sense of the change, the results were all normalized against the baseline value for comparison. The results of this parametric change are shown in Figure 24.

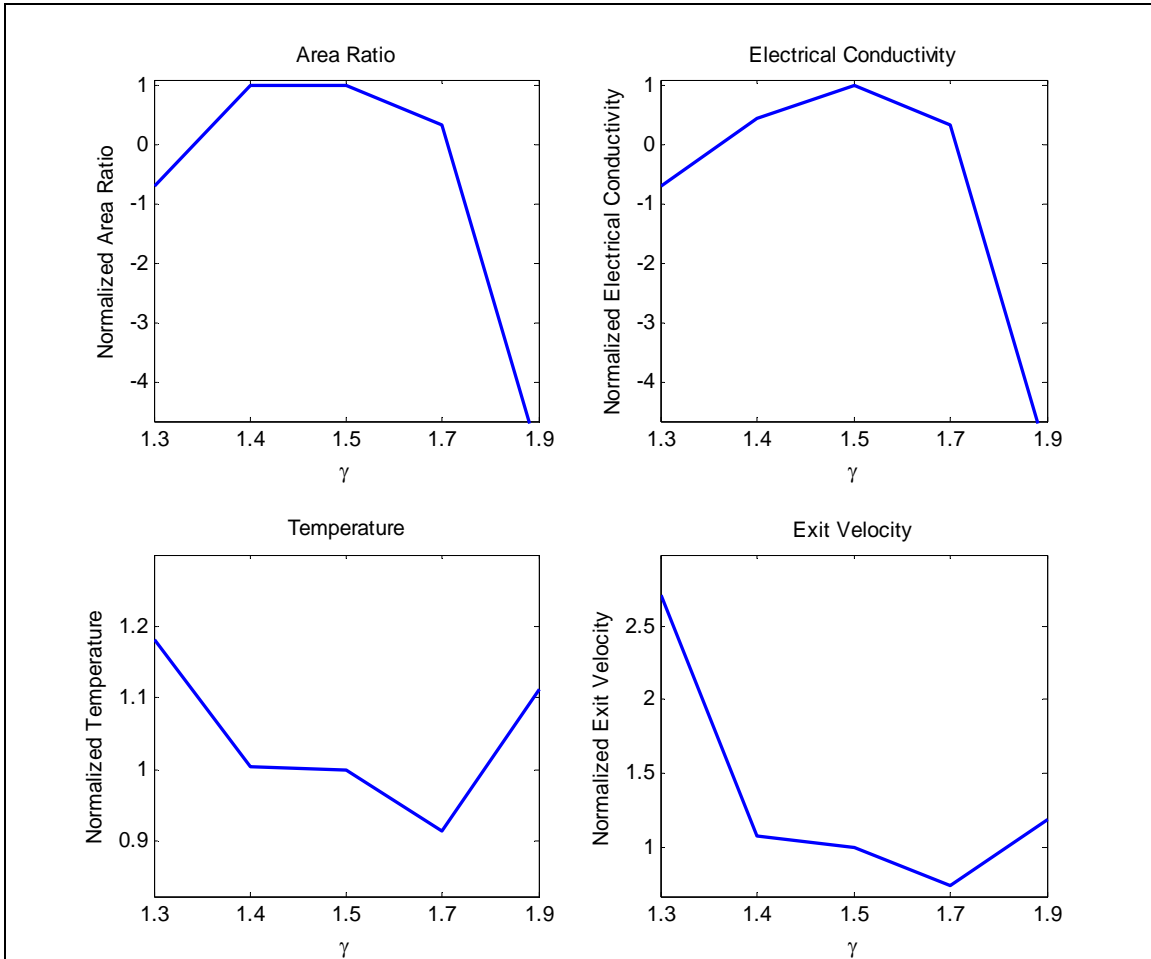


Figure 24. Variation of the Density of the Profile Frequency, γ .

The density of the profile frequency is a fractal parameter that has inconsistent results when the parameter is increased and decreased. In some instances, a decrease in γ results in a smoother, narrower frequency band, whereas in others, it yields a more jagged, wider frequency band. Increasing the profile frequency density has similar effects. Nonetheless, for the specific values of γ tested, the baseline profile had the most

randomness and variation throughout the profile and was chosen by Yan and Komvopoulos to be 1.5 for the best random fractal profile.

Of note in Figure 24 is that the shape of the curve for area ratio and electrical conductivity follow similar trends. Although a different shape than the area ratio and electrical conductivity curve, the temperature and exit velocity curves follow a similar trend as well. The unpredictable nature of the parameter γ has a direct effect on the similarly unpredictable results of the Pratikakis equation.

THIS PAGE INTENTIONALLY LEFT BLANK

VI. SUMMARY AND CONCLUSIONS

In this thesis, a computer program was developed to model nominally flat contact surfaces throughout the mechanism of contact. The use of analytical methods and Hertz contact theory allowed the program to solve for results analytically. Ultimately, a seemingly random profile is reduced to a finite number of Hertz contact problems that can be solved independently. By understanding each parameter of the fractal surface generator, one can tailor the surface to any known surface profile. Because many surfaces found in nature reveal surface profiles similar to fractal geometry, the application of this program has limitless potential.

A parametric study was conducted in order to further understand the fractal surface equation. A baseline was chosen based upon previous work by Yan and Komvopoulos, and the following parameters were varied: the number of superposed fractal ridges, fractal roughness, fractal dimension, and density of the profile frequency. The effects of changing each individual parameter were compared to the baseline and plotted.

The number of superposed fractal ridges had an effect on peak height, peak radius, and frequency band changes. Variation of the fractal roughness was determined to be a scale factor. The fractal dimension parameter had the greatest effect on peak height changes. The density of the profile frequency had inconclusive results.

Use of a preexisting electromagnetic rail gun program allowed application of the nominally flat contact surface results. The Pratikakis program clearly displayed the effects of surface profile upon performance of the electromagnetic rail gun. Each parameter was studied to determine its effects upon not only the surface, but the application to a real world problem. The parameters that were changed when analyzing the effect on profile shape were changed in the same manner when running the rail gun program, specifically increasing and decreasing the parameter from the baseline. The effect of each parameter had a direct effect on surface shape, which in turn changed the results of the rail gun program.

THIS PAGE INTENTIONALLY LEFT BLANK

VII. RECOMMENDATIONS

This research provides a method to model contact surfaces using a fractal equation. It simplifies the complicated problem of seemingly random contact down into a simple Hertz analysis. Although the problem is calculated on the three-dimensional level, it may be inaccurate in the fact that each contact peak is modeled independently. The effect that one peak has upon another may cause significant changes in the fractal surface and the way in which it reacts. Future studies using the finite element method would provide more accurate results. Also, a thorough validation of the model against any experimental test data would be beneficial to refine the program.

THIS PAGE INTENTIONALLY LEFT BLANK

LIST OF REFERENCES

- [1] S. Barros, "PowerLabs Rail Gun Research!," May 2007, <http://www.powerlabs.org/railgun.htm>, May 2008.
- [2] A. C. Ugural and S. K. Fenster, *Advanced Strength and Applied Elasticity*, 4th Ed., Upper Saddle River, N.J.: Prentice Hall, 2003.
- [3] J. A. Greenwood and J. B. P. Williamson, "Contact of Nominally Flat Surfaces," *Proceedings of the Royal Society of London. Series A, Mathematical and Physical Sciences*, Vol. 295, No. 1442 (Dec. 6, 1966), pp. 300-319.
- [4] J. F. Archard, "Elastic Deformation and the Laws of Friction," *Proceedings of the Royal Society of London. Series A, Mathematical and Physical Science*, Vol. 243, No. 1233 (Dec. 24, 1957), pp. 190-205.
- [5] W. Yan and K. Komvopoulos, "Contact Analysis of Elastic-Plastic Fractal Surfaces," *Journal of Applied Physics*, Vol. 84, No. 7 (Oct. 1, 1998), pp. 3617-3624.
- [6] P. Sahoo and N. Ghosh, "Finite Element Contact Analysis of Fractal Surfaces," *Journal of Physics D: Applied Physics*, Vol. 40 (21 July 2007), pp. 4245-4252.
- [7] J. Abdo and K. Farhang, "Elastic-Plastic Contact Model for Rough Surfaces Based on Plastic Asperity Concept," *International Journal of Non-Linear Mechanics*, Vol. 40, No. 4 (May 2005), pp. 495-506.
- [8] S. M. Ali and P. Sahoo, "Elastic-Plastic Adhesive Contact of Rough Surfaces Based on Plastic Asperity Concept," *Tribology Letters*, Vol. 22, No. 2 (May 2006), pp. 173-180.
- [9] N. Pratikakis, "Mathematical Modeling of Rail Gun," M.S. thesis, Naval Postgraduate School, Monterey, CA, 2006.
- [10] I. A. Polonsky and L.M. Keer, "A Numerical Method for Solving Rough Contact Problems Based on the Multi-Level Multi-Summation and Conjugate Gradient Techniques," *Wear*, Vol. 231 (1999), pp. 206-219.
- [11] G. Hu, P. D. Panagiotopoulos, Panagouli, O. Scherf, and P. Wriggers, "Adaptive Finite Element Analysis of Fractal Interfaces in Contact Problems," *Computer Methods in Applied Mechanics and Engineering*, Vol. 182 (2000), pp. 17-37.
- [12] *The New Encyclopedia Britannica*, 15th Ed., 2002, Vol. 4, s.v. "fractal", p. 915.

THIS PAGE INTENTIONALLY LEFT BLANK

INITIAL DISTRIBUTION LIST

1. Defense Technical Information Center
Ft. Belvoir, Virginia
2. Dudley Knox Library
Naval Postgraduate School
Monterey, California
3. Graduate School of Engineering and Applied Sciences
Naval Postgraduate School
Monterey, California
4. Young W. Kwon
Naval Postgraduate School
Monterey, California